



Thermo-rheological probe of microstructural evolution and degradation pathway in the flame-retarded PP/EVA/NOR/clay nanocomposites

Masoud Razavi¹ · Nazanin Sadeghi¹ · Seyed Hassan Jafari¹ · Hossein Ali Khonakdar^{2,3} · Udo Wagenknecht³ · Andreas Leuteritz³

Received: 21 May 2021 / Revised: 4 October 2021 / Accepted: 6 October 2021 / Published online: 25 October 2021
© The Author(s), under exclusive licence to Springer-Verlag GmbH Germany, part of Springer Nature 2021

Abstract

We perform comprehensive rheological and morphological investigations of multicomponent system of polypropylene (PP)/ethylene vinyl acetate copolymer (EVA)/Clay/N-alkoxy hindered amine type flame-retardant (NOR) in the presence of two types of compatibilizers. Effects of each component on the relaxation mechanisms were discussed in detail and correlated with the microstructural evolution governed by physical and chemical interactions between the components. Temperature sweep experiments indicated that in the blend nanocomposites, viscosity always increases by increasing temperature. This was found to be related to the migration of nanoclay in the system, originated from new thermodynamic state at the elevated temperatures. Differences in kinetics of morphological evolutions in the blend nanocomposites were explained based on the initial location of clay platelets, Stokes–Einstein relation in association with the rheological properties of the counterpart flame-retarded blend systems, and presence of chemical reactions. Moreover, enhanced miscibility/compatibility between PP and EVA phases at high temperatures was inferred from time sweep rheological data and then visualized using scanning electron microscope.

Keywords Rheology · Morphology · Filled polymer · Polymer blend · Relaxation time spectrum

Introduction

Polymers are a unique class of modern materials that provide numerous advantages such as strong mechanical performance and light mass density. Despite their various supremacies, polymers are weaker than conventional metals and ceramics in some aspects such as fire and chemical

resistance at elevated temperatures. As a result, various types of heat stabilizers (Murphy 2003b) and flame retardants (Murphy 2003a) have been developed in order to improve their drawbacks concerning high-temperature applications and flame resistance properties. Flame retardants and heat stabilizers can be organic or inorganic in their nature. It was indicated that the highest efficiency is achieved when a hybrid system of organic and inorganic additives is implemented (Hsiue et al. 2001; Qian et al. 2011; Tan et al. 2015; Yu et al. 2014). One of the problems associated with the conventional organic flame retardants such as aluminum hydroxide and magnesium hydroxide is their adverse effects on processability and mechanical performance of the host polymer (Guan et al. 2015; Sain et al. 2004; Zhao et al. 2017). In addition, application of some types of flame retardants such as halogenated compounds are limited/inhibited in the European Union and some parts of the USA due to their adverse environmental and health impacts (Aznar-Alemany et al. 2018; Blum et al. 2019; Hull et al. 2014; Shaw et al. 2010; Venier et al. 2015). Besides, some other types of heat stabilizers and flame retardants are chemistry

✉ Seyed Hassan Jafari
shjafari@ut.ac.ir

✉ Hossein Ali Khonakdar
hakhonakdar@gmail.com

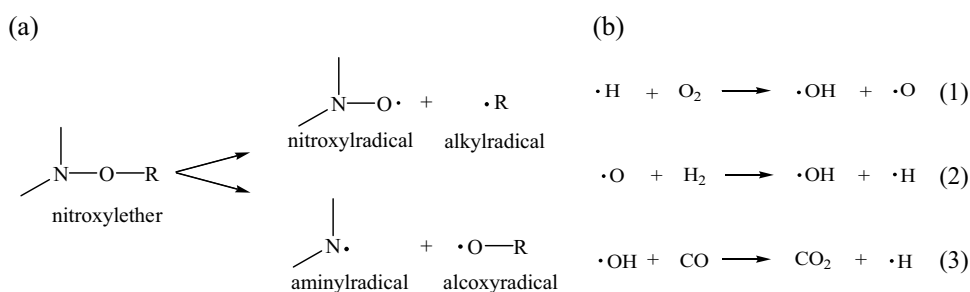
Masoud Razavi
razavi88@ut.ac.ir

¹ School of Chemical Engineering, College of Engineering, University of Tehran, P.O. Box 11155-4563, Tehran, Iran

² Iran Polymer and Petrochemical Institute, 14965/115, Tehran, Iran

³ Leibniz Institute of Polymer Research, 01069 Dresden, Germany

Scheme 1 **a** Degradation of nitroxylether groups. **b** Principal free radical reactions in the gas phase (flame); reaction 3 is the most exothermic one which can be suppressed by the generated free radicals from flame retardant degradation



specific, i.e., they will only be effective when added into a specific type of polymers (Hoang and Kim 2008; Schmitt 2007; Weil 1978; Yang et al. 2016). Thus, selection of an efficient flame retardant which can also pass the regulative rules is an important step in designing flame-retarded and heat-stabilized polymeric compounds.

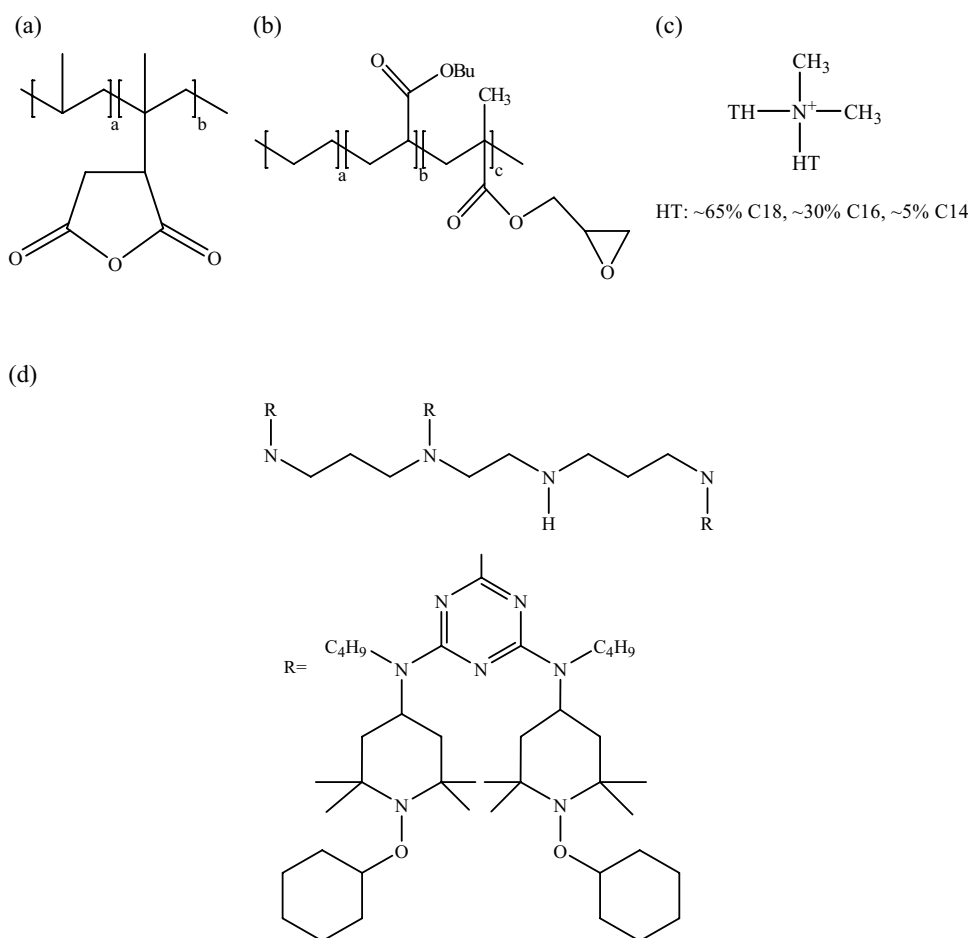
Among different types of polymers, polyolefins as the widely used commodity polymers have the largest share in applications such as home appliances, and cable and automotive industries (Galli 1999; Galli and Vecellio 2004; Sinclair 2001) where there is a high risk of fire and high temperature degradation (Tolinski 2015). In order to attain the desired properties, in most of these applications, polymers are used in blend form rather than individually. Blends of polypropylene (PP) and ethylene vinyl acetate copolymer (EVA) are among widely used polyolefin blends which offer a balanced stiffness/toughness mechanical properties (Faker et al. 2008; Razavi et al. 2015a). Studies regarding fire retardancy and heat stability of PP (Enescu et al. 2013; Seidi et al. 2020; Shao et al. 2014) and EVA (Bourbigot et al. 1999; Camino et al. 2000; Feng et al. 2015; Shi 2000; Szép et al. 2006; Yen et al. 2012) form an important area of the academic research in polymer science and technology. Numerous studies have been carried out over the years on the chemistry and processing aspects of PP/EVA flame-retarded and heat-stabilized multicomponent systems (Goodarzi et al. 2010; Rafiee et al. 2016; Ren et al. 2018). Recently, it has been found that N-alkoxy hindered amine which was conventionally used as a light stabilizer for polyolefins (Galbo et al. 2002; Winter et al. 1993), abbreviated as HALS (hindered amine light stabilizer) (Goedderz et al. 2020, Zhang et al. 2018), can significantly increase the fire resistance of polymers (Roth 2013). These flame retardants, commercially known as NOR (Goedderz et al. 2020; Nicolas et al. 2006; Pfaendner 2006, Roth 2013), contain nitroxylether groups which on degradation, produce highly reactive radicals (Scheme 1a) (Entezam et al. 2013). Those radicals can enter the gas phase and suppress the exothermic reactions (reaction 3 in Scheme 1b) (Green 1996; Lewin and Weil 2001) and thereby act as an efficient flame retardant. The mechanism of flame retardancy of these materials in the gas phase is similar to that of halogenated flame retardants; however, they do not contain any

halogenated and toxic compounds and are environmentally safe (Rault et al. 2015; Tirri et al. 2019). Another advantage of NOR is that as they are organic compounds, it is easy to process and mix them with polymers. Chemical structure of NOR 116, which has been used in this study, is shown in Fig. 1d. This flame retardant can also be effective in solid phase by causing extensive dripping and whereby protecting the polyolefin from flame (Klatt 2014). As mentioned before, flame retardant systems are usually introduced as a hybrid system of organic and inorganic mixtures into polymers where the synergistic effects can be expected (Wang et al. 2019; Xie and Qu 2001). Nanoclay has been found to be an effective inorganic additive that in addition to improving mechanical and barrier properties of polymers can also serve as an efficient flame retardant by influencing physical and chemical mechanisms in the solid phase (Beyer 2002; Kiliaris and Paspaspyrides 2010). Mechanism of flame retardancy of organo-modified nanoclay in PP has been studied in detail by Qin et al. (2005).

Flame retardant properties of PP, EVA, and their blend nanocomposites containing nanoclay have been extensively studied by introduction of different types of flame retardants. These studies mainly focus on thermal measurements, mechanisms of degradation in absence and presence of oxygen, and flammability and fire properties through fire retardancy experiments including limiting oxygen index (LOI) and cone calorimeter measurements (Dikobe and Luyt 2010; Haurie et al. 2007; Li and Qu 2003; Nie et al. 2013; Valera-Zaragoza et al. 2006; Wu and Qu 2001). The missing piece of all these studies is the microstructural investigations regarding the initial morphology in such a complex multicomponent system containing two polymeric phases (PP and EVA), flame retardant, nanoclay and possibly a compatibilizer which can be used to achieve uniform dispersion and distribution of different components and to improve interfacial properties between two polymeric phases. Also, evolution of viscosity and initial morphology in sublayers of the burning sample during temperature rising are other important aspects which need to be carefully investigated.

In this paper, we study the effects of N-alkoxy hindered amine (NOR116), as an environmentally friendly flame retardant, nanoclay, and two types of compatibilizers, on

Fig. 1 Chemical structures of **a** compatibilizer 1: polypropylene-graft maleic anhydride C₁, **b** compatibilizer 2: Elvaloy® PTW C₂, **c** organo-modifier of clay, and **d** flame retardant: NOR 116



the microstructure of the PP/EVA flame-retarded blend nanocomposites. Changes in viscosity, morphological, and rheological properties of the system over the wide range of temperatures, from room temperature to degradation onset, are precisely investigated. The study also provides a rich physical insight into the correlation between rheology and morphology of complex multicomponent polymeric systems, in addition to a specific case study on the PP/EVA/Clay/NOR blend nanocomposites.

Experimental

Material

PP (Moplen HP501H; density = 0.9 g/cm³, MFI at 230 °C and 2.16 kg = 2.1 g/10 min) from Basell, EVA (Escorene Ultra UL00218CC3; density = 0.94 g/cm³, MFI at 190 °C and 2.16 kg = 1.7 g/10 min, vinyl acetate content = 18 wt.%) from Exxon Mobile Chemical Company, Polypropylene-graft maleic anhydride (Polybond 3200, density = 0.91 g/cm³, MFI at 190 °C and 2.16 kg = 115 g/10 min)—which will be called compatibilizer 1, C₁ hereinafter—from

Chemtura, and Elvaloy® PTW (density = 0.94 g/cm³, MFI at 190 °C and 2.16 kg = 12 g/10 min) which is a terpolymer of ethylene, butylacrylate (BA) and glycidylmethacrylate (GMA)—compatibilizer 2, C₂—from DuPont, commercial nanoclay Nanofil® 5 (MMT-Na + modified with dimethyl, dehydrogenated tallow, quaternary ammonium) from Süd-Chemie, and a specific type of N-alkoxy hindered amine (NOR 116, M_w = 2261, melting range = 108–123 °C) from BASF which is specified as a new generation of eco-friendly flame retardants for polyolefins, were used in formulation of samples. Prior to melt blending, all the materials were dried for 16 h at 80 °C in a vacuum oven. Chemical structures of compatibilizers, organo-modifier of nanoclay, and flame retardant (NOR116) are presented in Fig. 1. Scheme 1 represents the degradation pathway of nitroxylether groups and mechanism of flame retardancy in NOR type materials.

Sample preparation

A twin-screw micro compounder MC 15 (Xplore, Netherland) was employed to mix all the components for 5 min under screw speed of 200 rpm. Set-point temperature for compounding was 190 °C. However, because of drifts in the

temperature and also shear heating during compounding, temperature can increase to 200 °C. The compounded materials were submerged in a cold-water pool and then dried in a vacuum oven at 50 °C for 24 h. The compositions of the prepared samples and their representative codes are presented in Table 1. Samples included pure PP, pure EVA, their pure blend, and also composites of PP/EVA with compatibilizer, clay, and NOR. Weight ratio of PP to EVA was kept equal to 75 to 25 in all the composites while weight percentage of other ingredients were varied between 2.5 and 5 wt. %.

Characterization

Morphology

Scanning electron microscopy and energy dispersive X-ray spectroscopy (SEM and EDX) Scanning electron microscopy (SEM; Cambridge S360, 20 kV, UK) was employed to characterize the morphology of blends, while energy dispersive X-ray spectroscopy (EDX) (Oxford Inca Energy350, UK) was used in order to determine the dispersion state of flame-retardant molecules. A compounded strand of each sample after proper drying was cryofractured in liquid nitrogen. Samples were then sputter coated with gold for good conductivity of electron beam prior to observation under the SEM–EDX.

Transmission electron microscopy (TEM) Transmission electron microscope (TEM; Philips EM208 microscope, 100 kV, Netherlands) was used to investigate the dispersion state of nanoclay and its partitioning between polymeric phases. The samples were microtomed at –120 °C.

Linear rheology

Dynamic rheometry in the melt state was carried out using stress-controlled rheometer (Anton Paar MCR301, UK) equipped with parallel plate geometry (diameter = 25 mm, gap = 1 mm). The samples were prepared as discs of 25-mm diameter and 2-mm thickness by compression molding at 200 °C. All measurements were done in a dry nitrogen atmosphere to suppress oxidative degradation. To achieve thermal equilibrium and structural relaxations, a waiting time after loading was applied before any measurement. Dynamic strain sweep data showed that rheological measurements performed at the strain of 5% safely fall within the linear viscoelastic limit of all samples. Rheological experiments were done in three different ways as follows:

- I. Dynamic frequency sweep experiment in the frequency range of 0.01 to 100 rad/s and fixed temperature of 200 °C.
- II. Temperature sweep experiment with the heating rate of 2 °C/min from 200 to 300 °C in the fixed frequency of 0.03 rad/s.
- III. Three-stage time sweep experiment at 290 °C as shown in Fig. 2. After this protocol, the sample was immediately submerged in liquid nitrogen and then cryofractured in order to observe its morphology at the elevated temperatures near its degradation onset. This experiment was performed with the aim of assessing the miscibility state of PP and EVA at the elevated temperatures.

Table 1 Composition and representative codes of the studied samples

Sample code	Composition (wt. %)					
	PP	EVA	PP-g-MA	PTW	Nanofil5	NOR116
PP	100	0	0	0	0	0
EVA	0	100	0	0	0	0
B	75	25	0	0	0	0
B/C ₁	71.25	23.75	5	0	0	0
B/C ₂	71.25	23.75	0	5	0	0
B/Nf5	71.25	23.75	0	0	5	0
B/NOR5	71.25	23.75	0	0	0	5
B/NOR5/C ₁	67.5	22.5	5	0	0	5
B/NOR5/C ₂	67.5	22.5	0	5	0	5
B/NOR-Nf5	71.25	23.75	0	0	2.5	2.5
B/NOR-Nf5/C ₁	67.5	22.5	5	0	2.5	2.5
B/NOR-Nf5/C ₂	67.5	22.5	0	5	2.5	2.5

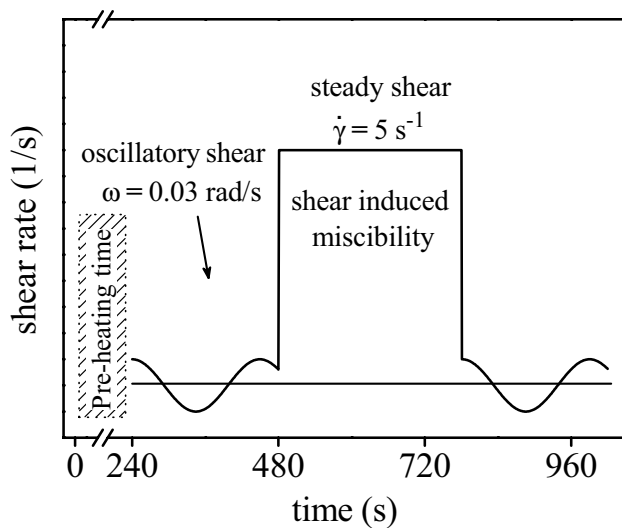


Fig. 2 Rheological protocol used to assess miscibility state of PP and EVA at the elevated temperatures

Thermogravimetric analysis (TGA)

To investigate thermal degradation of PP, EVA, and their blend, TGA measurements were performed under Nitrogen atmosphere using TGA analyzer (TA instruments, Q500). About 15 mg of each sample was heated from room temperature up to 700 °C with the rate of 10 °C/min.

Results and discussion

In analogy with the experimental section, the results and discussion part is arranged in the same order but with an additional sub-section (“[Comments on the origins of elasticity and relaxation in the multicomponent polymeric systems](#)”) to offer an experimentally driven view point on the origin of elasticity and relaxation in multicomponent polymeric systems.

Morphological studies

SEM was used to study the effect of different ingredients on the blend morphology, droplet size, size distribution, and dispersion quality of flame retardant in samples, while TEM were implemented to investigate the nanoclay morphology and its partitioning in the blend nanocomposites.

SEM

Figure 4a shows the morphology of neat PP/EVA 75/25 blend, in which EVA droplets are dispersed in the PP

matrix. Later it will be shown that all the other multicomponent samples have the same dispersed/matrix type of morphology, regardless of their composition. In order to have a better comparison between different samples and quantify the effect of different components on morphology, morphological parameters in terms of number average diameter (D_n), volume average diameter (D_v), and polydispersity (PD) of the droplet size of different samples, except for B/Nf5 sample in which EVA does not have droplet shape, were calculated according to Eqs. (1–3).

$$D_n = \frac{\sum n_i D_i}{\sum n_i} \quad (1)$$

$$D_v = \frac{\sum n_i D_i^4}{\sum n_i D_i^3} \quad (2)$$

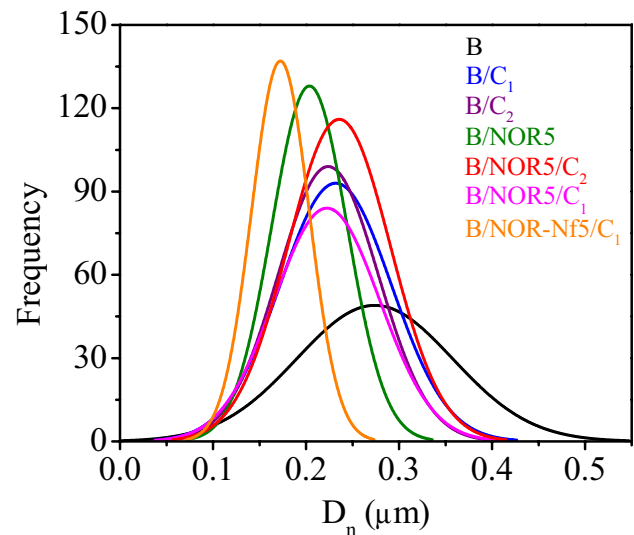


Fig. 3 Particle size distribution of different samples as fitted by normal distribution function. The Y-axis has been scaled by the number of measurements for an individual sample

Table 2 Morphological parameters of samples with droplet/matrix morphology: number average diameter D_n and polydispersity PD

Sample	D_n (μm)	PD
B	0.27	1.32
B/C ₁	0.23	1.24
B/C ₂	0.22	1.19
B/NOR5	0.20	1.11
B/NOR5/C ₁	0.22	1.22
B/NOR5/C ₂	0.24	1.18
B/NOR-Nf5/C ₁	0.17	1.10

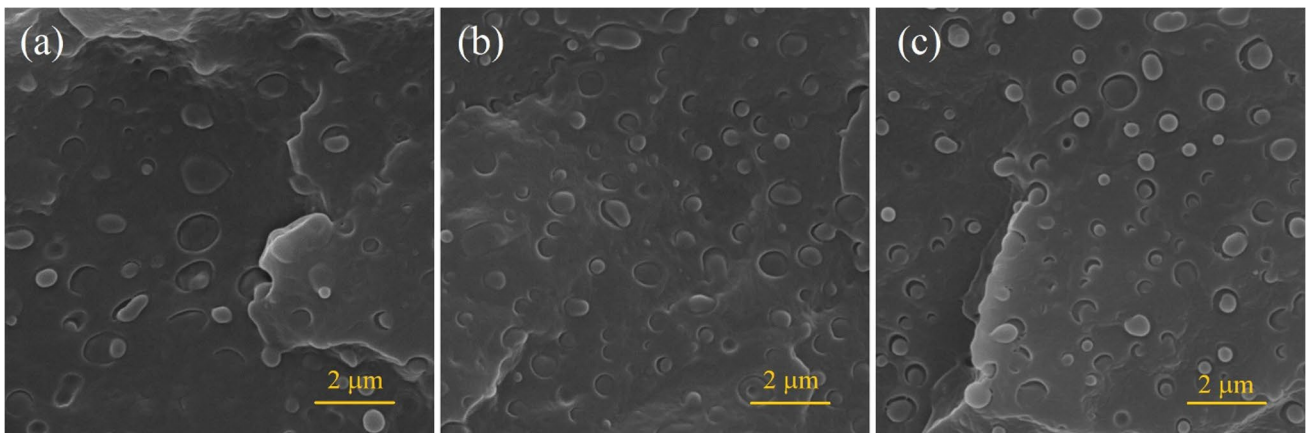


Fig. 4 SEM micrographs representing the effect of compatibilizer on the morphology of blend: **a** B, **b** B/C₁, and **c** B/C₂

$$PD = \frac{D_v}{D_n} \quad (3)$$

where n_i is the number of droplets having diameter D_i . Figure 3 shows the fitting of normal distribution function

(scaled by the number of measurements in each case) to the particle size distribution of different samples. It is seen that the different components meaningfully affected the morphology. To have a better comparison, values of D_n and PD as the two important parameters are tabulated in Table 2. It is

Fig. 5 SEM micrographs representing the effect of flame retardant and its simultaneous presence with compatibilizer on morphology of the blend: **a** B, **b** B/NOR5, **c** B/NOR5/C₁, and **d** B/NOR5/C₂

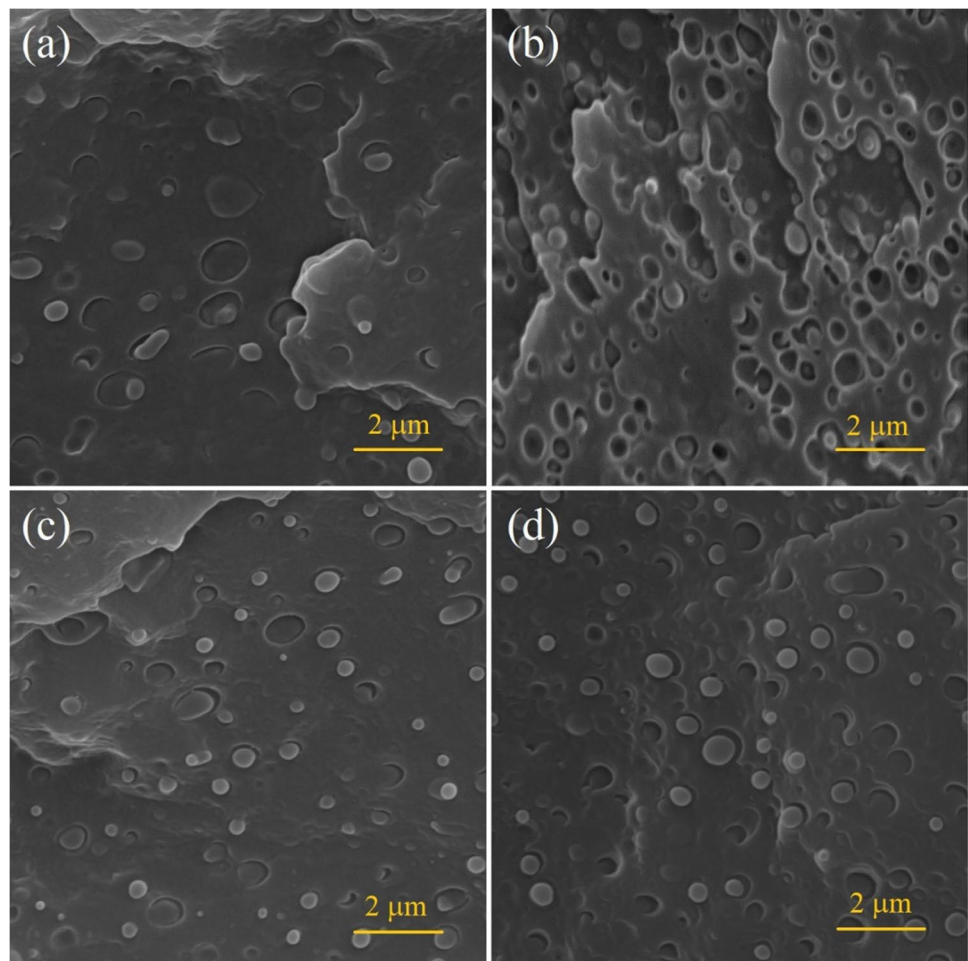


Fig. 6 SEM–EDX results indicating uniform distribution of flame retardant in the blend: **a** SEM of B/NOR5, **b** EDX spectra taken from EVA droplet, **c** EDX-spectra taken from PP matrix, and **d** EDX 2D-map of Nitrogen atoms

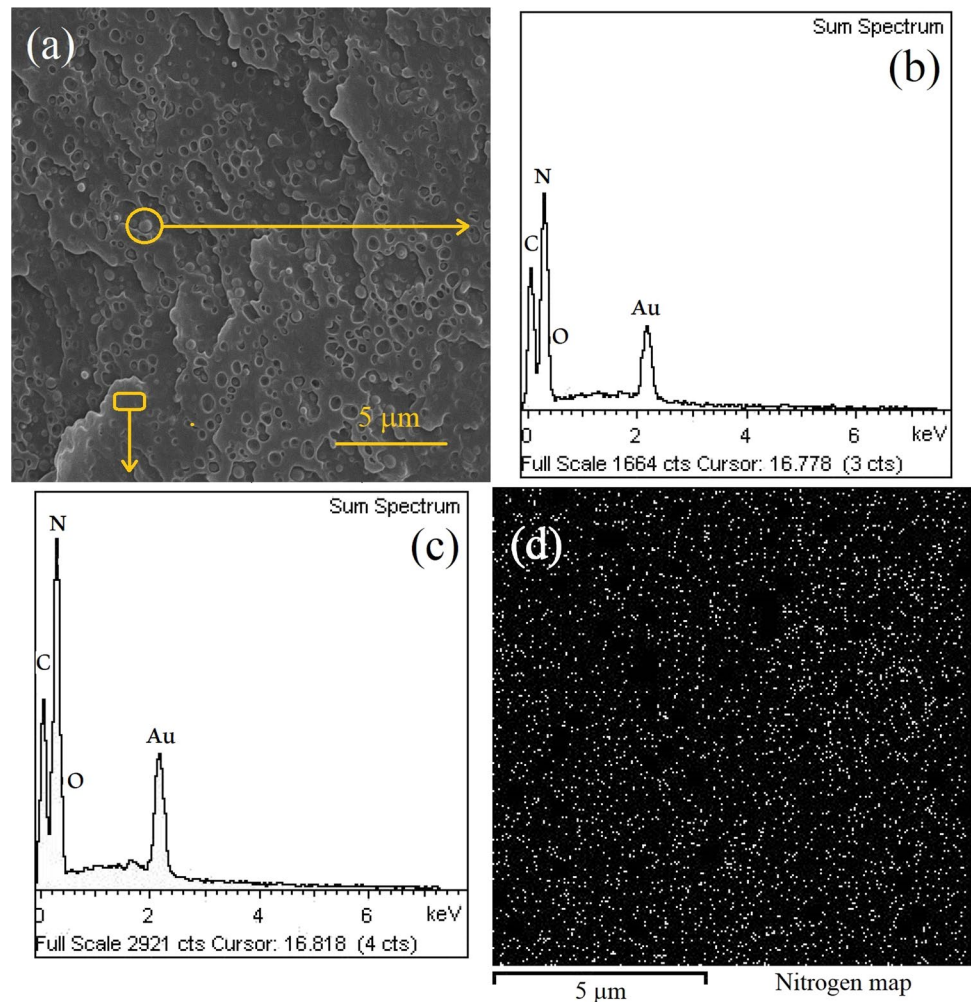
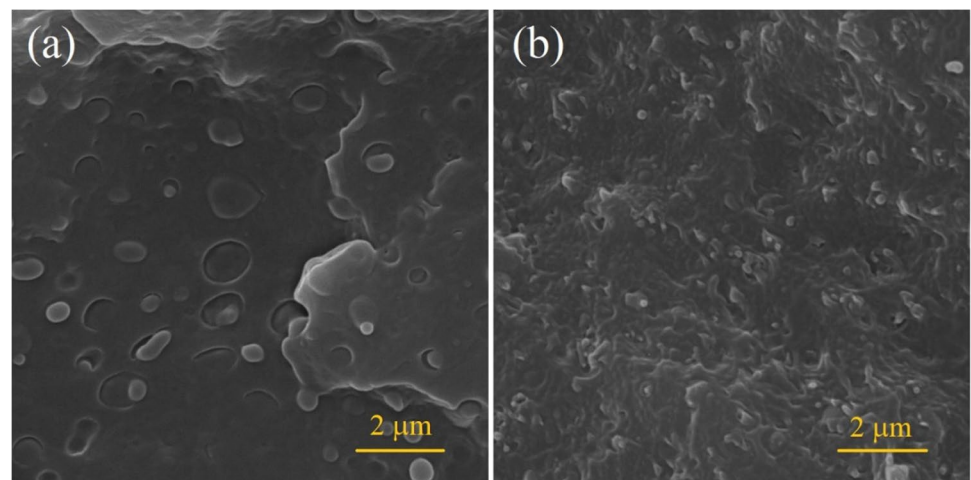


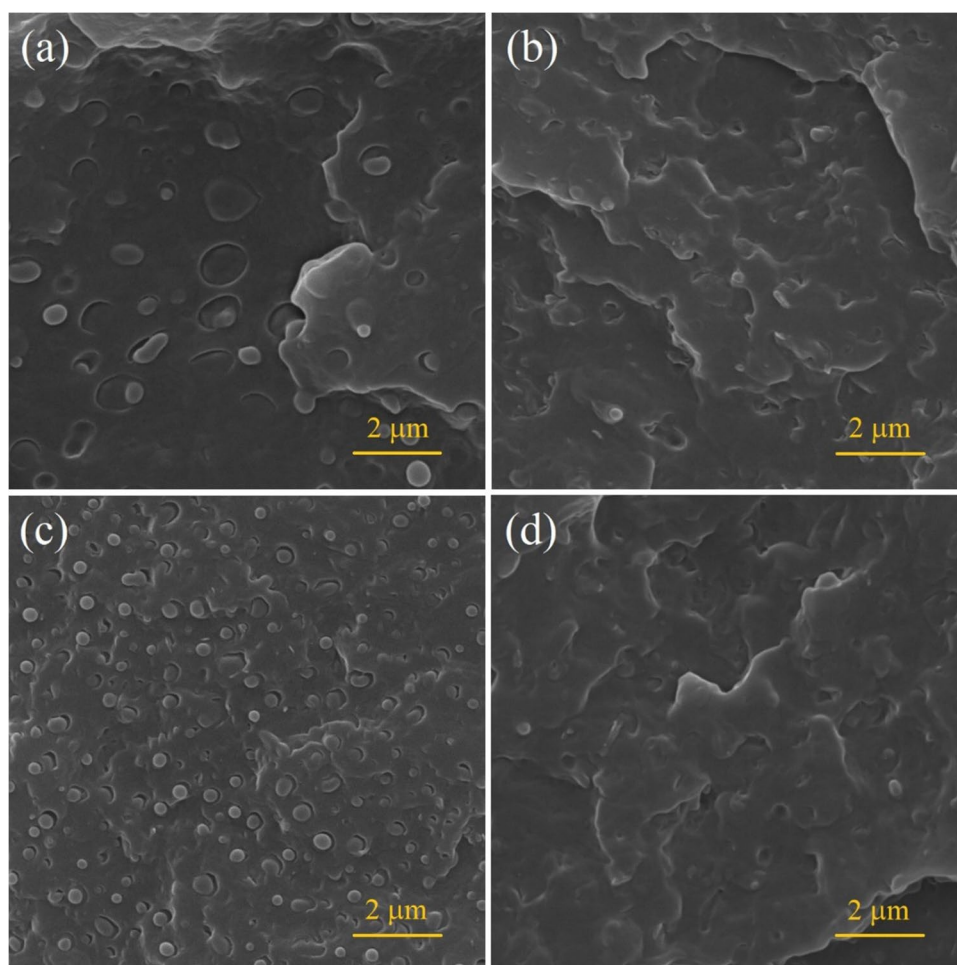
Fig. 7 SEM micrographs representing the effect of nanoclay (Nf) on the morphology of blend: **a** B and **b** B/Nf5



to be noted that extracting of the morphological parameters was based on large number of particles, ca. at least 150 particles, where SEM images with less magnification than what are presented in Figs. 4, 5, 6, 7, and 8 were considered in calculating D_1 values.

From Table 2 and SEM images of Fig. 4, it is seen that addition of C_1 and C_2 results in reduction of droplet size and improvement in size uniformity. Compatibilizers can migrate into the interphase during processing due to their chemical affinity to both phases (like dissolves like), and

Fig. 8 SEM micrographs representing the effect of simultaneous presence of nanoclay and flame retardant in the presence and absence of compatibilizer on the morphology of the blend: **a** B, **b** B/NOR-Nf5, **c** B/NOR-Nf5/C₁, and **d** B/NOR-Nf5/C₂



having relatively lower molecular weight compared to long polymeric chains and by reducing surface tension, they can result in reduction of particle size (Ajji and Utracki 1996). It can be inferred from the results that C₂ is more effective than C₁ in this regard. The reason behind higher compatibilization efficiency of C₂ will be discussed using the rheological measurements in the next sections.

The SEM images presented in Fig. 5 show the effects of flame retardant (NOR) in the presence and absence of the compatibilizers on the morphology of PP/EVA blend. Incorporation of NOR only to the blend results in reduction of particle size and its uniformity, similar to what have been seen for compatibilizer (Table 2). Plausibly, NOR molecules were initially localized in the matrix, but over the course of blending they migrate toward EVA, due to their more polar nature and chemical affinity to the EVA phase. Since the molecular weight of NOR is significantly lower than polymer, it is possible that its entry to the EVA droplets reduce the viscosity of dispersed phase and accordingly make it easier for the PP matrix to break up the EVA droplets to smaller sizes. Presence of NOR molecules in both phases is indicated in Fig. 6 where the EDX spectra taken from droplet

and matrix indicate the presence of Nitrogen atoms in both phases. EDX 2D-map of Fig. 6d demonstrates uniform distribution and dispersion in the sample.

NOR is more effective than C₁ and C₂ regarding reduction of particle size. But its effect is less significant when added simultaneously with compatibilizer. This can indicate that the compatibilizer prevents NOR concentration in EVA by promoting its uniform distribution in the system. Results of EDX for compatibilized flame-retarded samples (not shown here), i.e., B/NOR5/C₁ and B/NOR5/C₂, indicate a uniform distribution of flame retardant in the sample, similar to uncompatibilized one.

Prediction of nanoclay morphology and its partitioning in polymer blend nanocomposites have been systematically studied in the recent years (Razavi et al. 2016, 2017, 2018, 2015b). Partitioning of nano particles between different phases and their final location in a polymer blend nanocomposite are controlled via combination of thermodynamic and kinetic parameters (Razavi et al. 2018). Difference in polarity and interfacial tension of individual components are the key thermodynamic parameters while viscosity ratio of phases and mixing time are the governing kinetic

factors. Using Young's equation and geometric mean value of Wu (Razavi et al. 2018), wetting coefficient (the details of wetting coefficient calculation is presented in the discussions regarding temperature sweep rheological data in the section "Temperature sweep") of the system comprised of PP, EVA, and clay (Nanofil) at the processing temperature estimated to be equal to 0.89 (EVA is the second phase), implying that in the absence of any kinetical effect, clay (Nf) is preferentially localized at the interface with more tendency toward EVA phase. However, during the limited processing time, the thermodynamic equilibrium state may not be achieved. By introduction of clay into the blend in SEM images of Fig. 7, we can see that most of the EVA spherical particles disappear and some of them become very tiny in size. Similar change in morphology has been reported in the vicinity of phase inversion composition (Steinmann et al. 2001); however, in this case, the morphology change is barely related to phase inversion as the composition of blend is far away from phase inversion composition. The elongated morphology and disappearance of EVA particles circular shape could result from localization of clay nanoplatelets at the interface or inside the EVA domains. Reduction of size of dispersed particles is due to the compatibilization role of nanoclay which has been reported in other studies (Ammar et al. 2017; Salehiyan et al. 2016). The TEM results in the next section will verify the accuracy of our prediction about nanoclay location in the blend.

Simultaneous presence of flame retardant and nanoclay (NOR and Nf) refines the morphology more than before and generates a uniform morphology with hardly distinguishable boundary between the phases (Fig. 8b). The same effect is preserved when compatibilizer C_2 is added into the system (Fig. 8d). While, addition of compatibilizer C_1 into B/NOR-Nf5 retrieves the matrix-dispersed morphology again albeit with smaller dispersed phase domains. Recovering of drop-let-matrix type of morphology upon addition of C_1 could be a result of localization of the larger portion of nanoclay in the matrix compared to B/NOR-Nf5 and B/NOR-Nf5/ C_2 where higher portions of clay have been localized at the interface or EVA phase. Among the samples with spherical shape of dispersed phase, it can be inferred from Table 1 that B/NOR-Nf5/ C_1 has the finest EVA particle size. In addition to the compatibilization effect of C_1 , the localization of clay in the matrix and subsequent increased viscosity of this phase is an additional factor that inhibits the coalescence of EVA particles during processing and yields a finer morphology upon addition of C_1 to B/NOR-Nf5.

TEM

Nanoclay distribution/dispersion, intercalation/exfoliation state, and partitioning in the blend were directly visualized using TEM micrographs, shown in Figs. 9 and 10. In these

figures, each row illustrates the morphology of individual sample in three different magnifications. The scale bars are representative of length scale equal to 500 nm, 200 nm, and 100 nm, from left to right, respectively. The observed morphologies in TEM images are consistent with the predictions made using SEM micrographs in the preceding section. In Fig. 9 which is related to the B/Nf5, B/NOR-Nf5 and B/NOR-Nf5/ C_2 , it can be seen that clay platelets have a combination of intercalated and exfoliated states which are preferentially localized in the EVA domains and at the interface, as predicted. Because of clay localization in the EVA phase, elongated shape of clay platelets has been induced on the EVA domains. Red arrows indicate the presence of clay platelets inside the EVA domains and at the interface whereas, no clay particles are observed in the matrix.

In B/NOR-Nf5/ C_1 , unlike other nanocomposites, addition of C_1 into B/NOR-Nf5, as previously predicted from SEM results and can also be seen by the blue arrows in Fig. 10, results in localization of higher portions of clay platelets inside the matrix, and thus, constraining the entrance of nanofiller into the EVA domains. Consequently, as it was observed in Fig. 8c, the EVA phase appears as spherical domains unlike the other nano-filled samples, in which localization of clay inside EVA phase resulted in formation of elongated and non-spherical domains.

Rheology

Study of the linear rheological properties of polymeric multicomponent systems could be a powerful approach to acquire extensive knowledge regarding interaction of different components with each other and resulting morphology of the system. Moreover, at higher temperatures during flame where temperature of layers underneath the burning surface increases and sample melts and flows due to gravity (gravity mimics low shear rate deformation in the sample), measurement of rheological properties is important and can help us in material design and modeling of degradation and burning in polymers. The rheological data are studied in three main parts; first part aims to understand the microstructure of multicomponent systems and interactions of different components with each other through frequency sweep studies in the linear region. A major part of discussions is devoted to analyzing the relaxation spectra of samples. In the second part, temperature sweep measurement of rheological properties is performed with the aim to understand the rheological properties in the degradation pathway and evolution of microstructures and interaction of different components with each other. The final section is designated to attest the speculation which is made about the miscibility of PP and EVA at the elevated temperatures based on the changes in the interfacial tension of blend. Before proceeding to analyze

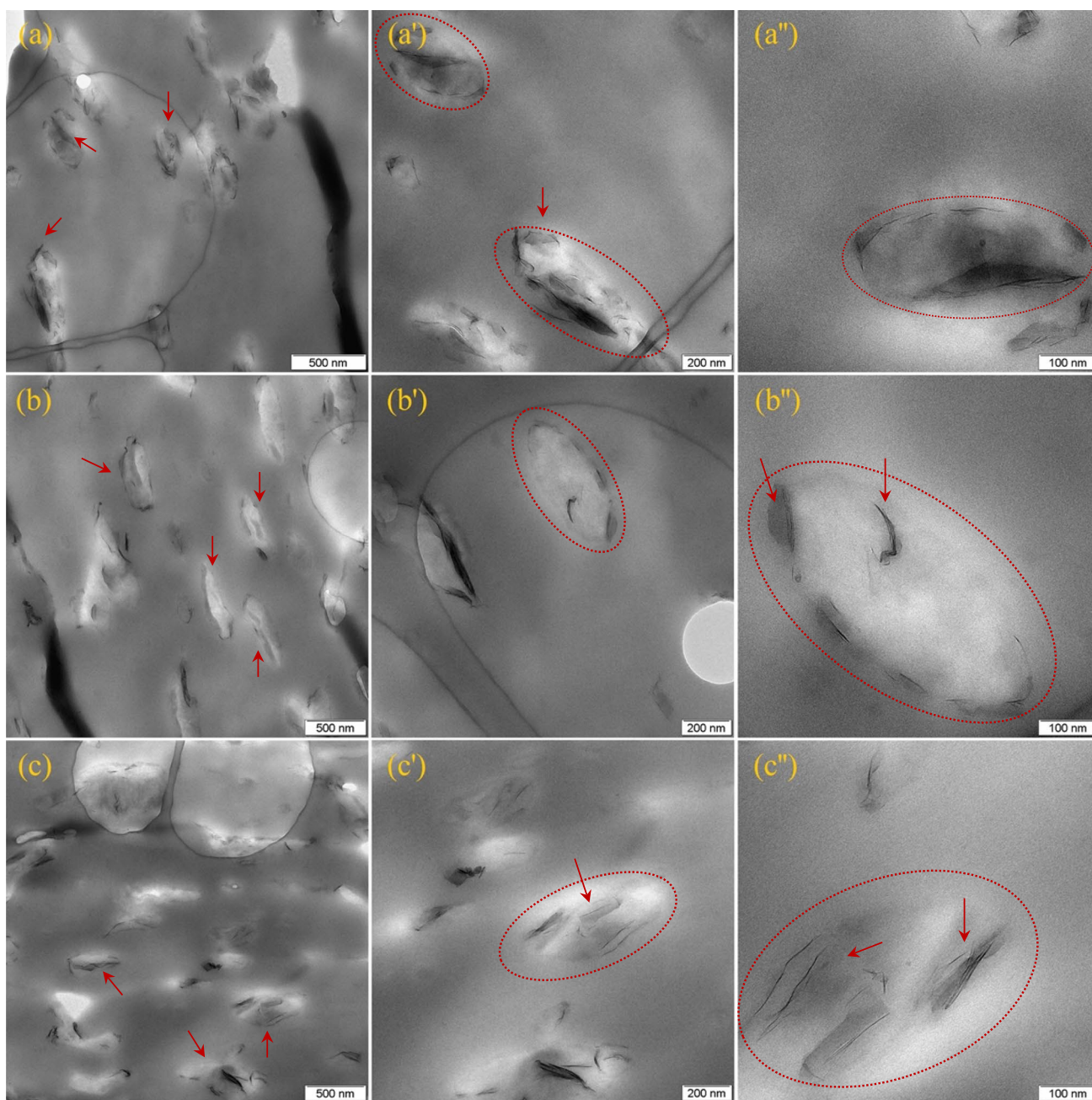


Fig. 9 TEM micrographs of **a, a', a''** B/Nf5; **b, b', b''** B/NOR-Nf5; and **c, c', c''** B/NOR-Nf5/C₂, at three different magnifications. Scale bars from left to right are indicative of distance equal to 500 nm,

200 nm, and 100 nm, respectively. Red arrows and dashed boundaries demonstrate the preferential localization of clay nanoplatelets at the interface or inside the EVA domains

the rheological data, we are going to have a separate section about the origins of elasticity and different types of relaxations in complex polymeric systems. This sub-section could be very informative regarding understanding the rheological properties of multicomponent polymeric systems and will significantly help us to precisely analyze the relaxation spectra of different samples.

Comments on the origins of elasticity and relaxation in the multicomponent polymeric systems

Different sources can contribute to the overall elasticity of a multicomponent polymeric system in the melt state (Razavi et al. 2016, 2018). Consider a multicomponent polymeric system composed of polymer 1, polymer 2, and filler. In such a system, there are other sources that determine the

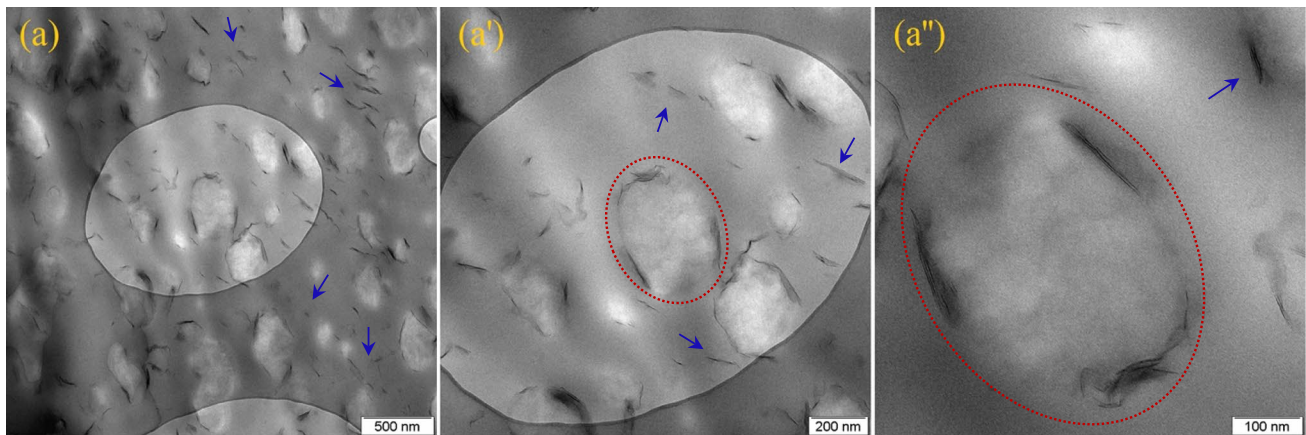


Fig. 10 TEM micrographs of B/NOR-Nf5/C₁ at three different magnifications. Scale bars from left to right are indicative of distance equal to 500 nm, 200 nm, and 100 nm, respectively. Blue arrows

show the localization of nanoclays at PP matrix and dashed boundaries indicate the clays localized at the boundaries. No clay is detectable inside the EVA domains

final magnitude of elasticity, in addition to the individual components. Generation of new interface/interphase (Lee and Park 1994) and possible existence of higher order structures could be the new sources of elasticity in this complex system (Almdal et al. 1992). Assuming a case where a small perturbation at the linear region, e.g. small amplitude oscillatory shear (SAOS) experiment, is exerted on a filled-multi-component sample, we could face the following phenomena:

- i. Relaxation of the polymeric chains at the bulk of individual polymer: this relaxation is not different from the relaxation of the single-phase polymer that takes place through reptation.
- ii. Relaxation of polymer chains at the interphase: the structure of the interphase depending on the compatibility/miscibility of the chains at this region or existence of reaction at the interface (e.g., in reactive compatibilization) could be significantly different from the bulk. Therefore, the chains at the interphase can have different relaxation times than in the bulk. In other words, a single chain at the interphase can relax in the media that its mean-field properties are different from the chain in the bulk.
- iii. Relaxation of the deformed particles: in an incompatible or immiscible blend, after removal of perturbation source, the deformed droplets of the dispersed phase return back to their original shapes (phenomenon known as shape relaxation (Bousmina 1999)), in order to minimize the free energy. The driving force that acts on the surface of a deformed droplet to push it back to its original shape depends on the interfacial area (size of particle) and interfacial tension. Therefore, the smaller the particle size and the interfacial tensions, the longer the time needed for shape relaxa-

tion to take place. An important conclusion is that at a constant droplet size, the shape relaxation time is longer in a compatibilized blend than in its non-compatibilized counterpart.

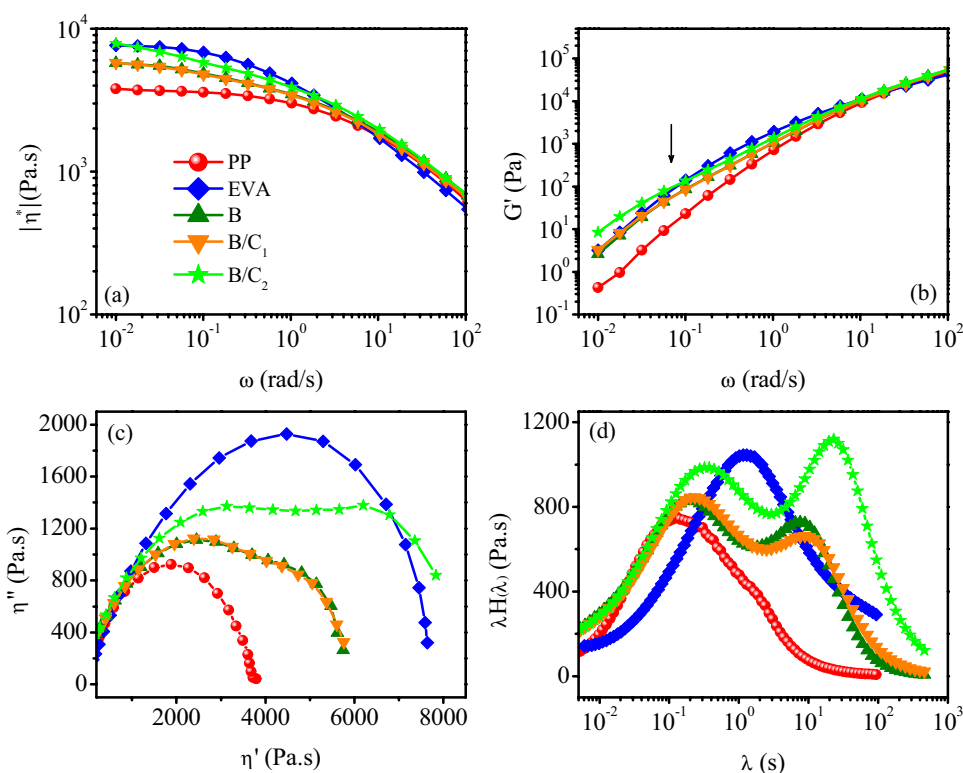
- iv. Relaxation of filler/polymer network: the direct connection of the filler particles to one another or their indirect connection through bridging chains can make a three-dimensional network of filler/polymer. The relaxation of chains involved in this network, or shape relaxation of the network as an individual unit, is the other types of relaxations that may exist in nanocomposites. However, it is usually impossible to experimentally observe these relaxations at the accessible time and temperatures of the rheological experiments.

Among the different types of relaxation mechanisms mentioned above, usually i has the shortest relaxation time, and in the absence of significant difference in the chain architecture and molecular weights between polymers, the bulk relaxation of the individual polymers take place at the comparable time scales. In the absence of reactive compatibilization, chains at the interphase relax at the time scale comparable to i, as well. Shape relaxation time is usually one to two orders of magnitudes longer than chain relaxation time. The longest relaxation time relates to the relaxation of the filler/polymer network, iv.

Frequency sweep

Figure 11a and b show the complex viscosity $|\eta^*|$ and storage modulus G' of the neat polymers and their blends in the absence and presence of two types of compatibilizers.

Fig. 11 Results of SAOS experiment of the neat polymers and blends in the absence and presence of compatibilizer: **a** complex viscosity $|\eta^*|$ vs frequency ω , **b** elastic modulus G' vs frequency ω , **c** Cole–Cole plot, and **d** relaxation spectrum, $\lambda H(\lambda)$ vs relaxation time λ



The neat polymers, PP, and EVA indicate typical linear melt behavior at the terminal region. Zero shear viscosity of EVA is higher than PP and its values for blends fall in between of corresponding pure components. For compatible and incompatible blends, it has been observed that when there is a notable viscosity difference between polymers, zero shear viscosity of blend has an intermediate value in between pure polymers, while when the viscosities of pure polymers are comparable, usually the viscosity of blend is higher than pure polymers and its curve locates above the curve of pure components (Kontopoulou et al. 2003; Wu et al. 2008). On the other hand, for miscible polymeric pairs with a comparable melt index, the viscosity of blend is always between the pure polymers (Hameed and Hussein 2004). At higher frequencies, viscosities of different samples are comparable due to the higher shear-thinning behavior of EVA and blend systems.

Storage modulus is a more sensitive material function that can highlight the structural differences of polymeric systems. It has been observed that polymer blends have higher elasticity at the terminal region and their behavior deviates from linear melt with dependency of $G' \sim \omega^2$. The increased elasticity of blend at this region is the consequence of shape relaxation, i.e., the relaxation of the droplets of dispersed phase. The relaxation times of the dispersed particles are usually longer than the reptation time of the individual polymer chains; therefore, by the time that polymer chains have already been relaxed through reptation, the unrelaxed

droplets keep the elasticity of the blend high and consequently less dependency of G' on ω at the terminal region is observed. The arrow on Fig. 11b indicates increased elasticity resulting from relaxation of the deformed dispersed phase. Addition of compatibilizer into the system results in higher elasticity. This effect is more pronounced when the blend is compatibilized with C₂ compatibilizer. Reduction of particle size and increased interaction between the phases at the interface are the two means by which addition of a compatibilizer can increase the elasticity at the lower frequency limit. As it was mentioned in the previous section, longer times are required for the smaller droplets to relax to their original shapes. This is due to their smaller surface areas and consequently less driving force from the interface to push them back to their original shapes. Alternatively, when there are strong interactions between phases at the interface, i.e., smaller interfacial tension, there will be less driving force to push the droplets back to their un-deformed states, and therefore, the shape relaxation time will be again longer. As it can be noticed from Fig. 11b, the shape relaxation in B/C₂ is more pronounced than in B/C₁. In SEM images, we observed that particle sizes of the dispersed phase in B/C₁ and B/C₂ are almost the same; therefore, the increased elasticity in B/C₂ compared to B/C₁ is mainly due to the difference in the quality of interface rather than particle size of dispersed phase. In other words, since the interfacial interactions in B/C₂ is stronger, i.e., less interfacial tension, so the shape relaxation time in this sample is longer than

B/C_1 , resulting in the larger elasticity of this sample in a same range of frequency. Calculation of interfacial tensions of blends based on morphological and rheological measurements, e.g., using Palierne emulsion model (Graebling et al. 1993; Razavi et al. 2018), could be very helpful for quantitative comparison of interfacial tensions between different samples; however, our focus in this study is on the phenomenological and qualitative aspects.

Cole–Cole equation and its corresponding plot are widely used for analyzing the dielectric data in materials science (Metzler and Klafter 2002). Similar approach was adopted to interpret SAOS rheological data by plotting imaginary viscosity $\eta'' = G''/\omega$ versus real viscosity $\eta' = G'/\omega$ (Friedrich and Braun 1992). This plot can also be used to visually assess the state of miscibility and compatibility in polymeric blends. For a single-phase linear polymer with a Maxwellian behavior, the Cole–Cole plot has semicircular (arc) shape (Han and Kim 1987) indicating the absence of complex relaxation mechanisms. The same shape is also observed for the miscible blends where the curve of blend is located between that of pure components. As it was mentioned in the section “Comments on the origins of elasticity and relaxation in the multicomponent polymeric systems,” different mechanisms can contribute to the elasticity of a multicomponent system. Those additional sources of elasticity will affect the shape of Cole–Cole plot in a particular way. In Cole–Cole plots of blend samples and corresponding polymers presented in Fig. 11c, it can be seen that curves of PP and EVA have semicircular shape. This indicates the presence of a single group of relaxation times in these samples. The two humps observed in the curves of the blend samples, from left (corresponding to higher frequencies) to right (corresponding to lower frequencies), are related to the bulk relaxation of chains in the blend and shape relaxation of dispersed phase, respectively. Presence of strong interactions at the interface of B/C_2 deviates the curve from arc shape and causes flattening and emergence of tail at the lower frequencies.

To get deeper insights into the relaxation of samples, discrete relaxation time spectrum for each sample is obtained by fitting generalized Maxwell model to the experimental storage G' and loss G'' moduli obtained from SAOS measurement by using Eqs. 4 and 5:

$$G'(\omega_j) = \sum_{i=1}^N H_i \frac{(\omega_j \lambda_i)^2}{1 + (\omega_j \lambda_i)^2} \quad (4)$$

$$G''(\omega_j) = \sum_{i=1}^N H_i \frac{\omega_j \lambda_i}{1 + (\omega_j \lambda_i)^2} \quad (5)$$

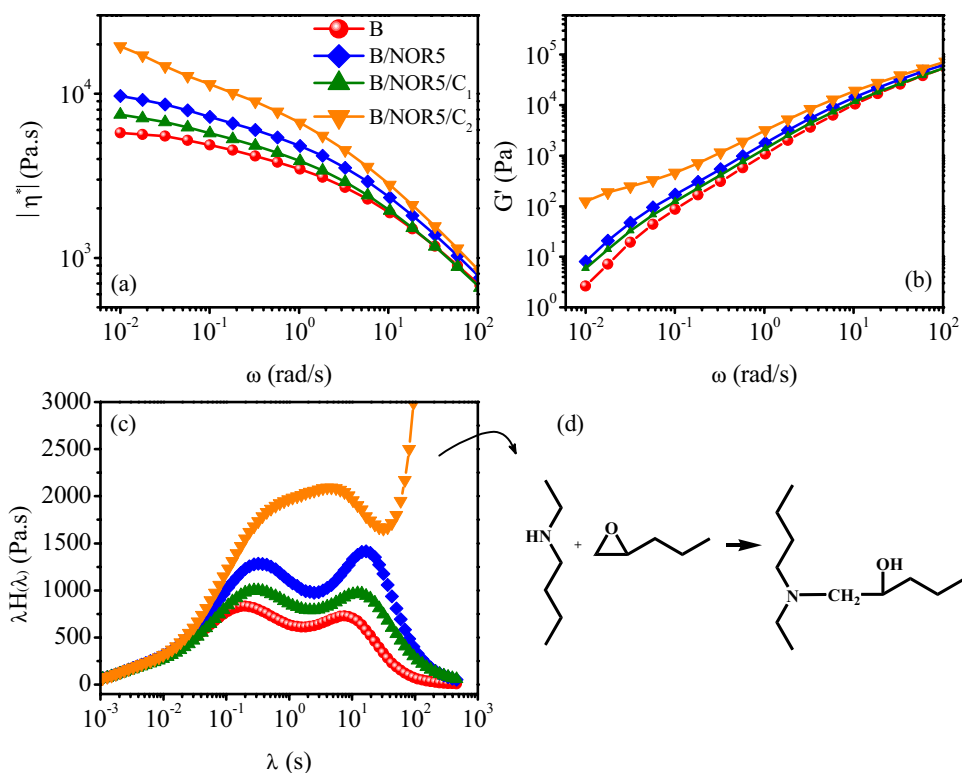
In these equations, H_i is elastic modulus corresponding to relaxation time of λ_i . In other words, H is the contribution

of relaxing species having the relaxation time of λ into the elastic modulus. Relaxation spectra are usually represented as $H(\lambda)$ vs λ or $\lambda H(\lambda)$ vs λ , where the X -axis is usually in log scale and Y -axis is in linear scale. In the latter representation, the Y -axis is multiplied by λ in order to magnify the relaxations at the long times that may have less contribution to the overall elasticity and may be harder to be detected in $H(\lambda)$ vs λ curve. The details of calculation of relaxation spectrum based on SAOS experiment have been presented in our previous publication (Razavi et al. 2017).

Figure 11d shows $\lambda H(\lambda)$ vs λ for the PP, EVA, and their non-compatible and compatible blends. Pure polymers have unimodal distribution of relaxation times indicating the presence of a unimodal distribution of molecular weight in the corresponding samples. The two peaks visible in the spectra of blend samples indicate two dominant relaxation mechanisms; the one at shorter times located between pure components relates to the relaxation of polymer chains at the bulk and interphase, which we will call it blend relaxation here in after, and another one at longer times is related to the shape relaxation of the dispersed phase. There is not much difference between relaxation spectrum of B and B/C_1 ; however, the shape relaxation time of the blend that is compatible with C_2 is significantly longer than other blends which as mentioned before, are related to the presence of strong interactions at the interface of this sample. As previously stated, $H(\lambda)$ shows the contribution of relaxing species having the relaxation time of λ into the elastic modulus. One should notice here that in Fig. 11d the heights of the peaks are displaying $\lambda H(\lambda)$, that is, the contribution of relaxing species with relaxation time λ into the elasticity is magnified by their corresponding λ ; therefore, in order to consider the absolute effect of each relaxing mechanism on elasticity of the system, one should exclude the effect of multiplication in λ . In other words, Fig. 11d presents higher peaks for shape relaxation than blend relaxation. However, after normalizing the heights with the corresponding relaxation times, the contribution of droplets into the overall elasticity should be much lower than the contribution of polymer chains.

Effect of NOR and its simultaneous presence with two types of compatibilizers on the rheological data are indicated in Fig. 12. Addition of NOR into the blend results in increase of viscosity and elasticity. The increase in elasticity/viscosity is lower when NOR is added to the blend together with C_1 (Fig. 12a and b). SEM images noted that the particle size in B/NOR is smaller than $B/NOR/C_1$. Smaller particle size, i.e., larger interface between two phases at a same concentration of dispersed phase, results in higher elasticity/viscosity of B/NOR compared to $B/NOR/C_1$. On the other hand, despite comparable particle size of $B/NOR/C_1$ and $B/NOR/C_2$, the latter has higher elasticity/viscosity than B/NOR . The increased elasticity/viscosity in $B/NOR/C_2$ can be due to the reaction between C_2 and NOR, and production of bulky

Fig. 12 Effects of NOR and compatibilizer on the SAOS data of neat blend: **a** complex viscosity $|\eta^*|$ vs frequency ω , **b** elastic modulus G' vs frequency ω , **c** relaxation spectrum, $\lambda H(\lambda)$ vs relaxation time λ , and **d** possible reaction resulted in species having very large relaxations times which is out of experimental window



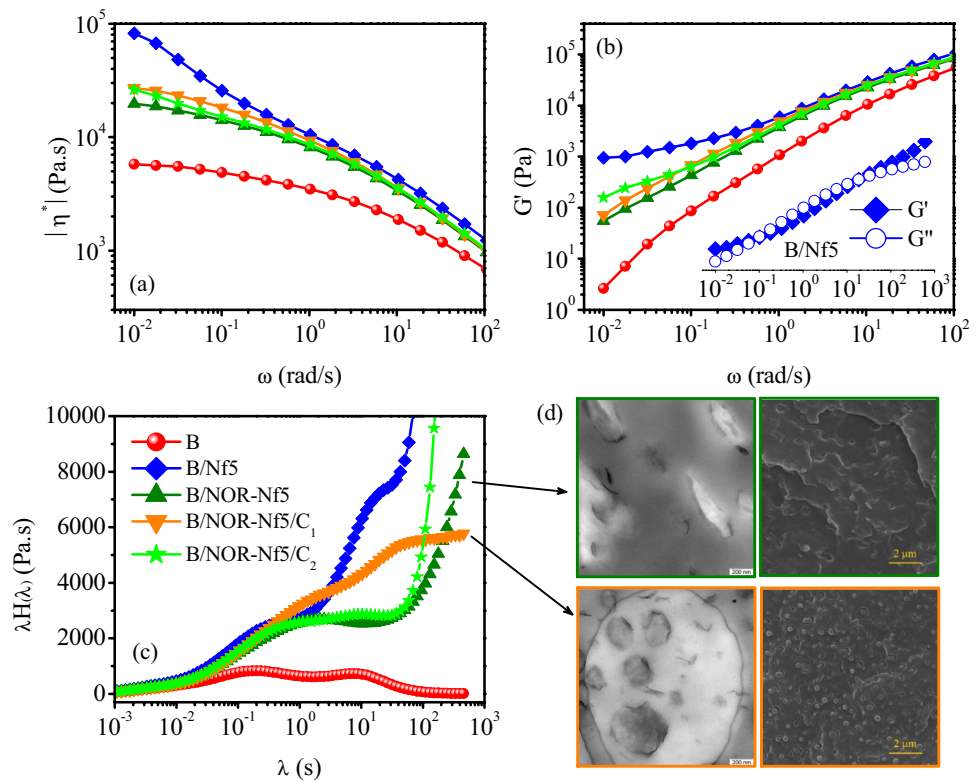
and high molecular weight chains. The secondary amine in NOR and epoxy group of C_2 , as it is indicated in Fig. 12d, can react with each other. Reaction between tertiary amines of NOR and epoxy groups in C_2 is also possible; however, the steric hindrance of bulky groups in NOR may decrease the probability of such reactions.

A better insight regarding interactions between different phases and components of compatibilized flame-retarded samples is feasible using relaxation time spectra in Fig. 12c. Similar to blend, B/NOR5 and B/NOR5/ C_1 both have two peaks: one representing the relaxation of chains and the other one denoting shape relaxation. Both of the peaks have a slight shift to the longer relaxation times which in the case of first peak is due to the higher interaction between phases after addition of NOR and C_1 and in the case of second peak is due to the reduction in the size of dispersed phase. And as it can be noticed, the shift of second peak to longer times is slightly higher in B/NOR5 than B/NOR5/ C_1 . The height difference between various samples relates to their viscosity differences. An interesting behavior is observed when NOR and C_2 are simultaneously presented. In this case, the peaks of polymer chains and shape relaxation of dispersed phase converge together and merge into one wide peak with a plateau in between. An enormous increase in the tail of $\lambda H(\lambda)$ curve at longer times is also noticed. The appearance of tail with large $\lambda H(\lambda)$ values is indicative of generation of new relaxation mechanism with a very large relaxation time that is not possible to observe their peak

at the experimental time window. In order to monitor the aforementioned peak, one needs to run the experiment for longer times (lower frequencies). The emergence of the new relaxation mechanism with long relaxation times is related to the reaction between NOR and C_2 chains, and generation of bulky and high molecular weight new species. Generation of these new molecules could induce more restrictions on the reptation of linear PP and EVA chains and accordingly move the bulk relaxation peak to longer relaxation times. Meanwhile, the shape relaxation in B/NOR5/ C_2 is affected in a way that the dispersed particles relax faster compared to the other flame-retarded samples, i.e., B/NOR5 and B/NOR5/ C_1 . Shorter shape relaxation time for B/NOR5/ C_2 compared to B/NOR5/ C_1 and B/NOR5 is intelligible due to larger particle size of B/NOR5/ C_2 (Table 2). On the other side, despite smaller particle size of B/NOR5/ C_2 compared to the neat blend B, it can be perceived that the shape relaxation time in this sample is shorter than neat blend. The reason of this apparent discrepancy could be the difference in the interfacial tension between B and B/NOR5/ C_2 . It was reported that the increase in molecular weight results in an increase in polymers surface tension (Park et al. 2007). In B/NOR5/ C_2 , the interfacial tension can increase as a result of generation of new molecules with high molecular weight, and consequently, we can observe shorter shape relaxation time in B/NOR5/ C_2 in comparison to the neat blend.

Figure 13a and b demonstrate the effect of concurrent presence of different components on the viscosity and

Fig. 13 Effects of presence of clay (Nf), NOR, compatibilizer on the SAOS data of the neat PP/EVA blend: **a** complex viscosity $|\eta^*|$ vs frequency ω , **b** elastic modulus G' vs frequency ω , **c** relaxation spectrum, $\lambda H(\lambda)$ vs relaxation time λ , and **d** TEM (left column) and SEM (right column) of B/NOR-Nf5/C₁ (upper images) and B/NOR-Nf5/C₂ (lower images) rationalizes the observed significant difference at relaxation spectra of these samples



elasticity of the blend. Addition of 5 wt. % nanoclay into the blend has the highest effect on increasing elasticity and viscosity of the system. It has been reported that the complete independency of G' from frequency is an indication of generation of filler network in nanocomposites. So, as a consequence, G' stays above G'' curve in all the frequency ranges, known as solid-like behavior. By comparing G' and G'' curves of B/Nf5 (inset image of Fig. 13b), it can be seen that the two curves cross each other at lower frequency region and G' increases over G'' ; however, it does not stay completely above G'' curve. This behavior is a representation of the fact that in this nanocomposite, the filler network is about to get established but despite higher elasticity, the network has not been fully created yet. Elasticity of B/NOR-Nf5/C₂ is slightly higher than B/NOR-Nf5/C₁ and B/NOR-Nf5. Despite close elasticity and viscosity of B/NOR-Nf5/C₁ and B/NOR-Nf5, deviation of the behavior from liquid-like in the latter is more than former which is due to the higher concentration of filler near the interface and inside the EVA domains where there is higher possibility of generation of filler network whereas in B/NOR-Nf5/C₁ fillers are sparsely distributed at the interface and matrix.

Comparison of relaxation time spectra between these samples in Fig. 13c can provide more details regarding microstructure of samples. Three groups of relaxation times for B/Nf5, B/NOR-Nf5, and B/NOR-Nf5/C₂ and two groups for B and B/NOR-Nf5/C₁ are observed. As previous, the smallest relaxation peak is related to the bulk relaxation of

polymeric chains in PP and EVA. In the case of samples with nanofiller (Nf), the dominant relaxation peak of first group of relaxations has been shifted to the longer times. This effect is a result of interactions between polymeric chains and filler, and consequent slowdown of the chain dynamics. The second relaxation mechanism is related to the relaxation of dispersed phase. For B, B/Nf5, B/NOR-Nf5, and B/NOR-Nf5/C₂, this relaxation time is in the same order. Compatibilizing effect of nanoclay has been widely reported in the polymer blend nanocomposite (Razavi et al. 2015b). Although the interface of EVA domains in B/Nf5, B/NOR-Nf5, and B/NOR-Nf5/C₂ is covered by Nf and it is expected to observe a delay in their relaxation time, but the deformation, i.e., distortion from un-deformed state during oscillatory test, of the EVA domains, is probably not as strong as the deformation of spherical domains in the neat blend. Therefore, less deformation of the elongated EVA domains could compensate over slower relaxation of the compatibilized interface in these samples. On the contrary, the second relaxation of B/NOR-Nf5/C₁ has been significantly increased compared to the neat blend. As it can be noted from the SEM and TEM micrographs and Table 2, the average size for the EVA spherical particles in this sample is the minimum among all the other samples. Also, since less filler has been localized at the interface of these samples, therefore, no significant compatibilization effect from nanoclay is expected. In addition, there are very small particles that can significantly push the shape relaxation of the disperse

particles to the longer times. Therefore, a slow and tailed relaxation of dispersed phase is observed for this sample, where the tail could relate to the less perfect filler network. Unlike B and B/NOR-Nf/C₁, all the other nanocomposites demonstrate huge increase in $\lambda H(\lambda)$ at long times. In these three samples, as it was observed in the TEM images, nanoclays mainly localize at the interface and dispersed phase; thus, a rigid network of filler/polymer is generated. Generation of strong physical network can significantly enhance the relaxation time beyond that of experimental window. In B/NOR-Nf5/C₂, the onset of huge increase in $\lambda H(\lambda)$ is earlier. This is primarily because of the existence of another enhancing mechanism, which is the reaction between NOR and C₂. Figure 13d correlates the interesting contrast observed between relaxation spectra of B/NOR-Nf5/C₁ and B/NOR-Nf with that of the nanoclay localization and morphology of samples. It indicates how the migration of nanoclay toward matrix as a result of presence of C₁ can affect the morphology of sample and the associated relaxation spectrum.

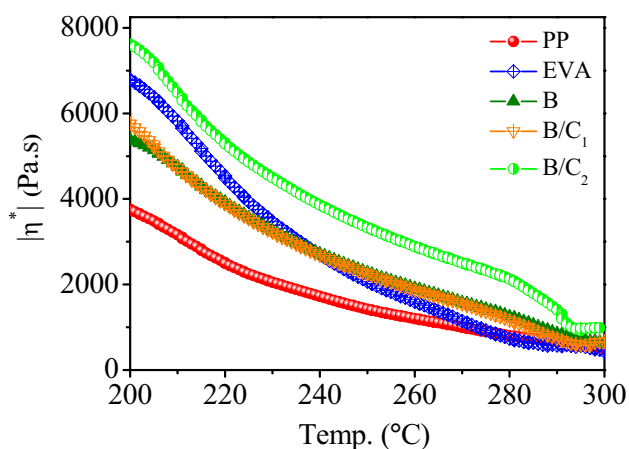
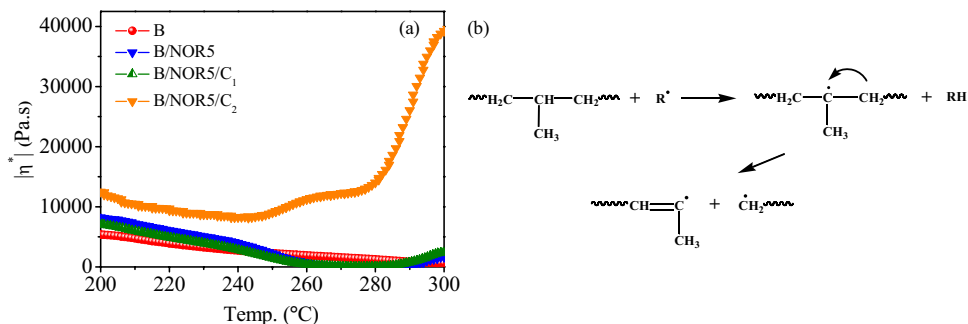


Fig. 14 Complex viscosity $|\eta^*|$ vs temperature of neat polymers and blends in the absence and presence of compatibilizer

Fig. 15 a Effects of NOR and compatibilizer on the complex viscosity $|\eta^*|$ vs temperature. **b** A possible reaction between radicals of NOR and PP that results in viscosity reduction around 250 °C for B/NOR5 and B/NOR5/C₁



Temperature sweep

Temperature sweep rheological experiments were performed aiming to study viscosity changes in the bulk of samples during temperature increase that happens over the course of degradation and burning of polymer. Figure 14 shows the complex viscosity vs temperature for neat polymers along with their uncompatibilized and compatibilized blends. The viscosity of all samples decreases uniformly with increasing temperature. Viscosity values are around 500 Pa s near 300 °C. This viscosity is equivalent to the viscosity of melt at 200 °C when it is under 100 rad/s oscillatory shear. To gain better sense of these values, one can think of a tomato paste which has viscosity around 250 Pa s at room temperature.

Effect of NOR and its simultaneous presence with compatibilizer on the viscosity of blend is shown in Fig. 15a. Degradation of nitroxyl groups of NOR can take place around 250 °C as it was indicated in the Scheme 1a. The resulting highly reactive radicals can extract tertiary hydrogens from PP chains and facilitate its thermal degradation. The reaction between radicals of NOR and PP (shown in Fig. 15b) takes place around 250 °C and causes the viscosity to drop to as low as 20 Pa s, which is approximately the viscosity of chocolate syrup at room temperature. The same effect is also observed when NOR is added to the blend together with C₁. This significant drop in viscosity is probably due to the flame retardancy mechanism of NOR which is known as extensive dripping. The viscosities of B/NOR5 and B/NOR5/C₁ decay until 285 °C and then start to increase. This upturn in viscosity was not observed for the neat (B) and compatibilized blends (B/C₁ and B/C₂) in Fig. 14. Therefore, the increase in viscosity at higher temperatures for B/NOR5 and B/NOR5/C₁ could be the result of the reaction between NOR and other components in the system. In these samples, NOR can act as a crosslinker through its multiple reactive sites of amine groups. In the case of B/NOR5/C₂ viscosity starts to increase around 250 °C after an initial decay, then stays constant and finally around 280 °C upsurges to the larger values. As previously noted in the discussions regarding frequency sweep data of B/NOR5/

C₂ (Fig. 12c and d), the reaction between epoxy groups of C₂ and NOR molecules could be another possible reaction in this sample that can result in increase in the molecular weight. Therefore, presence of these reactions outweighs over the adverse effect of the degradation of NOR on the molecular weight of PP. Viscosity of B/NOR5/C₂ is more or less constant between 265 and 280 °C. This could stem from the balanced effect of PP degradation and branching of NOR and C₂ molecules. The second increase in viscosity, but with a delay and less amplitude, is also observed for B/NOR5/C₁ and B/NOR5. The severe increase in the viscosity of B/NOR5/C₂ at the second step, in addition to the reaction of epoxy groups of PTW (C₂), could be a result of the reaction between ester groups of C₂ and NOR that is facilitated at higher temperatures.

Introduction of clay into the blend results in an unexpected increase of viscosity with increasing temperature independent of presence of other components such as compatibilizer or flame retardant (Fig. 16a). This is particularly evident in the sample with the highest clay content, i.e., B/Nf5. One may initially think that the presence of some chemical effects such as reaction between modifier of filler and polymeric phases is responsible for the observed phenomena, but considering the unreactive nature of organo-modifier of Nanofil (Fig. 1c), this hypothesis is invalidated. Therefore, the observed behavior must be originated from some physical changes associated with nanoclay, during the temperature raise in the system.

The preferential localization of filler in a polymeric blend can be predicted according to the difference between interfacial tensions of the individual blend components. The method is based on the fact that every loaded polymeric blend tends to reach a minimum interfacial energy (Bagheri-Kazemabad et al. 2012). Young’s equation (Eq. 6) (Davoodi et al. 2016, Gomari et al. 1989), evaluating the wetting coefficient (ω_a) at thermodynamic equilibrium, is mainly used to estimate the position of filler (here organoclay) in a blend nanocomposite:

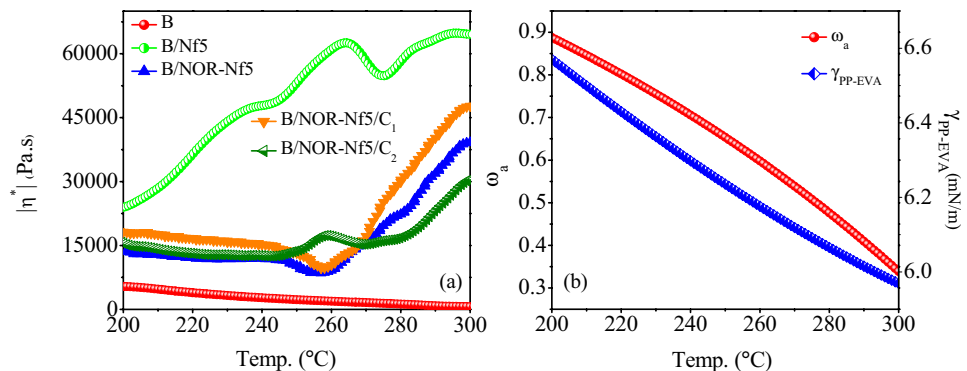
$$\omega_a = \frac{\gamma_{\text{clay-A}} - \gamma_{\text{clay-B}}}{\gamma_{A-B}} \tag{6}$$

Here $\gamma_{\text{clay-A}}$ and $\gamma_{\text{clay-B}}$ are interfacial tensions between clay and polymer A and B, respectively, and γ_{A-B} is the interfacial tension between polymer A and B. For wetting coefficients higher than 1 clay will be located in polymer B, while for the amounts lower than – 1 clay will be selectively distributed in polymer A, and it will be located mainly at the interface of two phases if the coefficient has values between 1 and – 1. For $0 < \omega_a < 1$ localization will be at the interface but with more tendency to phase B, and for $-1 < \omega_a < 0$ it will be at the interface but with more tendency to phase A. The interfacial tension between components can also be calculated from their surface tensions using the geometric mean equation of Wu (Eq. 7) (Bagheri-Kazemabad et al. 2012, Gomari et al. 1989):

$$\gamma_{1-2} = \gamma_1 + \gamma_2 - 2 \left[\sqrt{\gamma_1^d \gamma_2^d} + \sqrt{\gamma_1^p \gamma_2^p} \right] \tag{7}$$

where γ_1, γ_2 are surface tensions of components 1 and 2, γ_1^d and γ_2^d represent the dispersive parts of the surface tensions of components 1 and 2, and γ_1^p and γ_2^p stand for the polar parts of the surface tensions of components 1 and 2, respectively. The surface tension values of polymers at a specific temperature can be obtained by linear extrapolation of literature values using the related temperature coefficients. Considering EVA as polymer 2 in Eq. 6, we calculated ω_a in the temperature range of 200–300 °C (shown in Fig. 16b). It should be noted that the wetting coefficients in Fig. 16b have not been experimentally measured. They have been extrapolated using temperature coefficients based on the interfacial data at room temperatures (Gomari et al. 1989, Hosseiny et al. 2020; Picard et al. 2007; Razavi et al. 2018; Roe 1965). However, they can provide a rough estimation of the trend of variations in ω_a values versus temperature. This parameter shows that clay (Nf) does not have strong preferential tendency to the individual polymeric phases, so in the absence of kinetic effects, it prefers to locate at the interface with

Fig. 16 **a** Effects of presence of clay (Nf), NOR, and compatibilizer on the complex viscosity $|\eta^*|$ vs temperature. **b** Evolution of the wetting coefficient ω_a of Nf, and interfacial tension γ_{PP-EVA} with temperature



slightly higher tendency to the EVA phase. This prediction is in complete agreement with the experimental TEM observations of Fig. 9a. Regardless of the accuracy of the absolute values of wetting coefficient in Fig. 16b, the trend of variations of this parameter is decreasing with increasing temperature. This implies that by increasing temperature, tendency of filler to PP phase increases. Therefore, there is a possibility of migration of clay platelets from interface and EVA domains towards PP phase. This can provide uniform dispersion and distribution of filler platelets in the blend. The evolved filler morphology can positively contribute to the changes of viscosity with temperature. The heating rate during temperature sweep is 2 °C/min, so it will take 50 min to reach from 200 to 300 °C. This can provide enough time for the clay platelets to migrate in the blend. For other samples, B/NOR-Nf5, B/NOR-Nf5/C₁, and B/NOR-Nf5/C₂, after an initial decrease of viscosity, an increase in viscosity similar to the one observed for B/Nf5 is noticed. The less clay content in these samples can be responsible for the delayed increase in viscosity.

Since G' is more sensitive to the morphological changes, we compared normalized G' (regarded to G' value at 200 °C) of different samples in Fig. 17. This representation provides better comparison of the morphological evolution. As it can be concluded, the trend of changes in elasticity is increasing for all the samples, representing the occurrence of clay migration from beginning, at 200 °C. In the case of B/NOR-Nf5 and B/NOR-Nf5/C₁, there is a minimum in elasticity before it starts to increase sharply at around 260 °C. As discussed in the results of Fig. 15, as a result of generation of active radicals of NOR molecules, PP chains are degraded

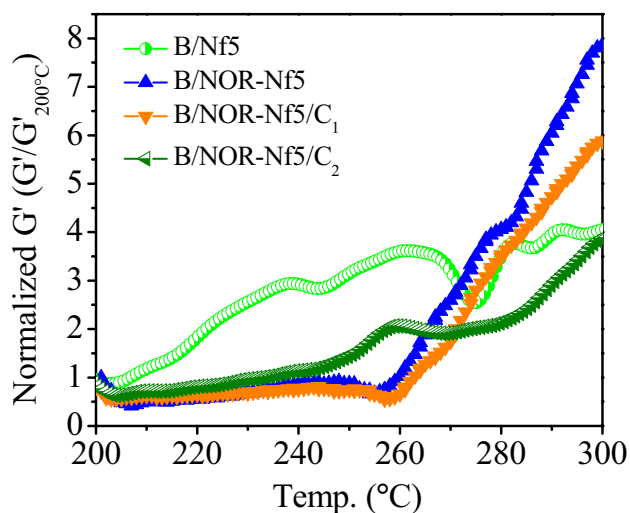


Fig. 17 Comparison of the elasticity change between nanocomposites during temperature sweep SAOS experiment. Storage moduli have been normalized regarding the storage modulus of each sample at 200 °C

in the matrix. In B/NOR-Nf5 and B/NOR-Nf5/C₁, the minimum in elasticity/viscosity is due to the same effect. However, after degradation of the polymer chains in matrix, since the viscosity of polymer chains around clay platelets significantly decreases, therefore clay platelets diffuse with significantly faster rate. This faster migration results in steep change in the normalized G' values of B/NOR-Nf5 and B/NOR-Nf5/C₁ in Fig. 17. On the other hand, in B/NOR-Nf5/C₂, the reactions of NOR and C₂ which mainly take place at the interface increase the local viscosity and therefore make it harder for clay platelets to migrate toward PP matrix. As a consequence in this sample, we observe sluggish increase in elasticity vs temperature as compared to B/NOR-Nf5 and B/NOR-Nf5/C₁. Sharper increase of elasticity in B/NOR-Nf5 compared to B/NOR-Nf5/C₁ is due to the higher concentration of the filler at the interface and EVA domains in B/NOR-Nf5, while in B/NOR-Nf5/C₁ a main portion of clay platelets is already localized in the matrix. To put it in another way, greater contrast between concentration of filler at the interface/EVA domains and matrix in the case of B/NOR-Nf5 compared to B/NOR-Nf5/C₁ generates more driving force for the Fickian (Berthier et al. 2004) and non-Fickian (Hallinan Jr et al. 2010, Rehage et al. 1970) diffusion of the clay platelets in the blend. To have a better insight about the effect of surrounding medium viscosity on the filler diffusion, we can consider Stokes–Einstein relation $D_{SE} = k_B T / f \pi \eta R$ (Zwanzig and Harrison 1985), where η is the pure solvent viscosity, T is the absolute temperature, k_B is the Boltzmann constant, and f is a constant depending on the hydrodynamic boundary conditions (B.C.) at the solute surface; stick B.C. $f=6$ or slip B.C. $f=4$. As suggested by this relation, the diffusion coefficient is inversely proportional to the viscosity of solvent. Considering the viscosity contrast between B/NOR5 and B/NOR5/C₂ at ca. 270 °C (70 Pa s for B/NOR5 and 12,300 Pa s for B/NOR5/C₂), we can roughly estimate that the diffusion coefficient of clay can be 180 times higher in B/NOR-Nf5 than in B/NOR-Nf5/C₂. Besides, in low molecular weight polymers—in our case, degraded chain in B/NOR-Nf5—real diffusion rate can be up to 200 times higher than the predicted values by Stokes–Einstein relation when the size of filler is smaller than the polymer chain radius of gyration R_g (Liu et al. 2008).

Miscibility analysis and time sweep

In addition to the interesting observation regarding the changes in the viscosity/elasticity of different samples, we are curious to realize the effect(s) of increasing temperature on the miscibility of PP and EVA phases. The decreasing trend of the interfacial tension between PP and EVA γ_{PP-EVA} (shown in the right-hand side of Fig. 16b) implies the possibility of increased compatibility between these polymers at higher temperatures. To achieve deeper insight regarding

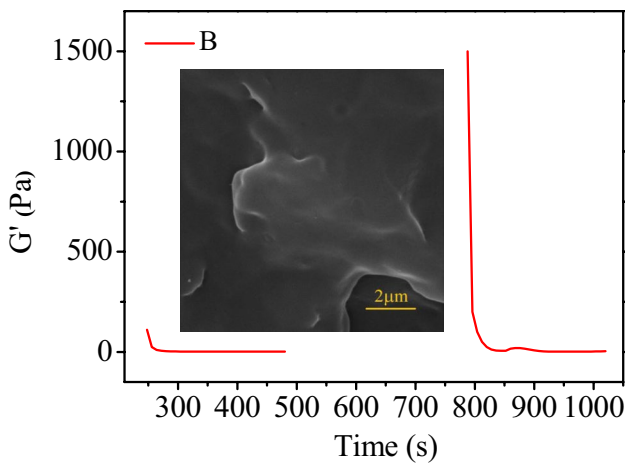


Fig. 18 Elastic modulus G' vs time for 75/25 PP/EVA blend at high temperature (290 °C) obtained in the SAOS experiment based on a protocol which has been visualized in Fig. 2. The inset SEM image depicts the morphology of sample at the temperature of the rheological experiment

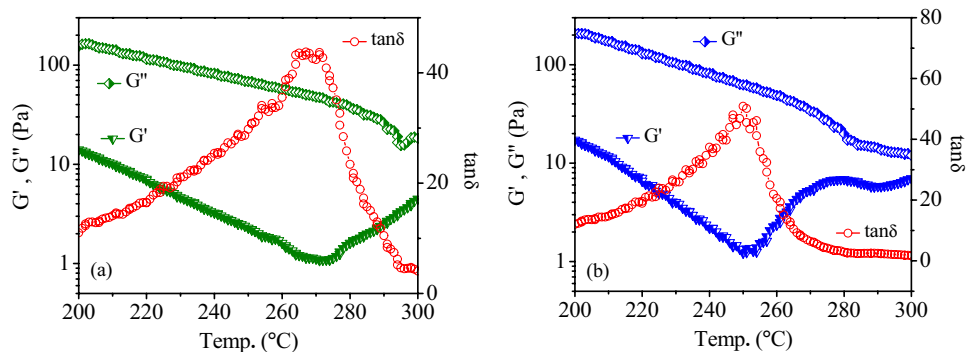
high temperature miscibility of PP and EVA, we tested the blend under the rheological protocol of Fig. 2 at 290 °C. In order to observe the blend morphology at high temperatures using SEM, the melt between parallel plates of rheometer was quenched into liquid nitrogen immediately after finishing the experiment. During oscillatory experiment (shown in Fig. 18), the elastic modulus G' are in the same order before and after high shear and remain constant over time. The constant elasticity vs time indicates that at this temperature, morphology of blend has been already established and does not evolve over time. The inset SEM image of Fig. 18 visualizes the established morphology of PP/EVA 75/25 blend at high temperature (290 °C). SEM image and G' data demonstrate that higher compatibility and miscibility for PP and EVA blend are achieved at higher temperatures and accordingly the matrix dispersed morphology disappears, so we observe a uniform morphology. Likewise literature reports about miscibility of EVA and polyethylene PE (Hemmati et al. 2013, 2014a, b) and other polyolefin pairs (Niu and

Wang 2006), we observed a similar enhanced compatibility at higher temperatures for the specific case of PP and EVA.

Dynamic rheological experiments have been identified as an indirect method to probe morphological changes and phase separation in polymer blends (Kapnistos et al. 1996; Sharma and Clarke 2004; Vlassopoulos et al. 1997). In these studies, a single-phase miscible polymer blend is quickly brought into unstable or metastable region in its phase diagram, in order to measure the kinetics and mechanism of phase separation; at the same time, evolution of rheological material functions is measured over time. To determine the phase transition temperatures, material functions are measured versus temperature over the course of temperature change from miscible region toward unstable or metastable region. At the phase transition temperatures some characteristic changes appear in the associated curves. The main qualitative conclusions of the kinetic studies are as follow: when the phase separation results in co-continuous structures through spinodal decomposition, the elasticity at of lower frequency region in SAOS experiment decreases over time. On the other side, development of dispersed droplet phase leads to an increase in elasticity at low frequencies (Vinckier and Laun 1999). Two competing behavior is observed in the temperature ramping experiments; Elasticity decreases by increasing temperature and moving away from T_g due to the associated increase in mobility. On the contrary, in the vicinity of phase separation temperature, thermodynamic forces appear, and the elasticity of the system increases due to the generation of new interfaces. Therefore, phase transition region is usually detectable as a slope change in the elasticity vs. temperature curve (Kapnistos et al. 1996).

Having the brief background in the preceding paragraph, now we are interested to monitor the temperature dependency of the SAOS material functions in PP/EVA 75/25 blend (at a fixed low frequency) when, unlike previous studies, the sample is heated form phase-separated region at 200 °C toward higher temperatures (Fig. 19a). By increasing temperature, elasticity decreases due to increase in chain mobility. Around 270 °C an unexpected upturn appears in G' being the indication of enhanced elasticity. One may initially

Fig. 19 Storage G' and loss G'' moduli and loss tangent $\tan\delta$ vs temperature for **a** PP/EVA 75/25 blend and **b** EVA



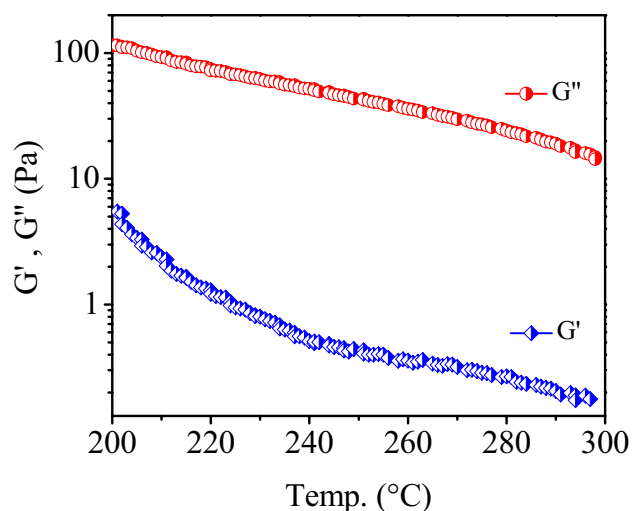


Fig. 20 Storage G' and loss G'' moduli vs temperature for PP

correlate this increased elasticity with phase separation in the system. However, the direct morphological observation in the inset SEM image of Fig. 18 suggests the reverse, i.e., at higher temperatures the blend is more homogenous rather than being immiscible. This puzzling contrast is resolved by checking the same parameters for the pure EVA in Fig. 19b in which a similar trend is noticeable for the pure EVA. On the other hand, this feature is absent for the pure PP as it is seen in Fig. 20.

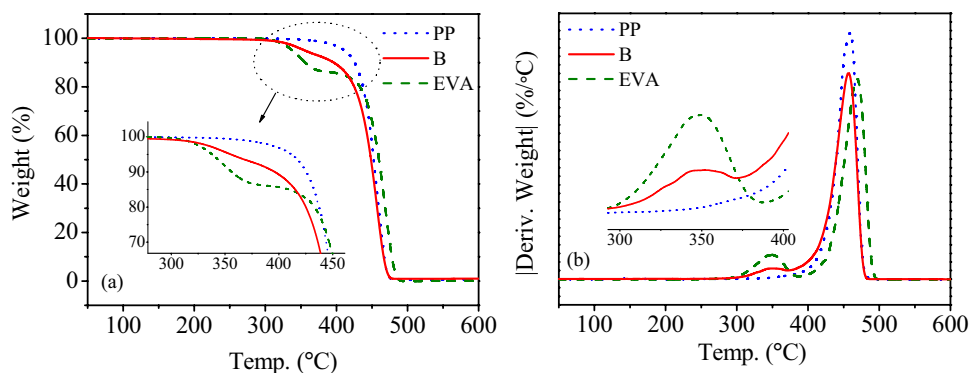
There are several studies on the EVA/PE blends (Hemmati et al. 2014b, 2015) and their nanocomposites (Hemmati et al. 2013, 2014a) which associate the similar changes in the slope of G' curve of blend to the phase transition temperatures. In these studies, some changes in the slope of G' curve are observed, instead of a sharp minimum. Such behavior may not necessarily be a sign of phase transition and can essentially be the same effect that we spotted here but with a smaller amplitude. The difference in the amplitude of the change in the slope of G' curve in our study and other reports could be related to the difference in the content of vinyl acetate groups, molecular weight of polymers, and

structure of the copolymer. Detailed characterization needs to be done in order to understand the origin of such transition in the rheological data. Our preliminary investigations based on TGA data in Fig. 21 shows that the degradation onset temperatures for EVA and blend are much lower than that for PP. It was indicated that EVA has two-step thermal degradation process with the earlier one onseting around 300 °C and relating to the loss of acetic acid and formation of double bonds and free radicals in the main chain (Costache et al. 2005). Physical or chemical association of such degraded structures might be the reason for increase in the elasticity and peak at $\tan\delta$ in EVA and the neat blend. The transition temperatures detected by rheological data are around 30 °C and 50 °C lower than degradation onset detected by TGA for the neat blend and EVA, respectively. This could be because of the slower temperature ramping in rheological measurements (2 °C/min) compared to temperature ramping at TGA measurements (10 °C/min) and more sensitive nature of rheological measurements compared to thermogravimetric measurements. The delayed rheological transition in the neat blend compared to pure EVA could be due to the lower concentration of EVA chains in blend.

Conclusion

In-depth studies were conducted on the effects of different components including compatibilizers, nanoclay, and flame retardant (NOR) on the morphology and rheology of PP/EVA 75/25 blend. Correlations were established between the initial morphology of sample, studied by SEM and TEM techniques, and frequency sweep small amplitude oscillatory shear rheological properties. We offered a universal discussion on the origins of elasticity and relaxation mechanisms in the multicomponent polymeric systems by detailed analysis of PP/EVA/Clay/NOR/Compatibilizer system. Presence of reactions between compatibilizer and NOR was found to result in tremendous increase of viscosity which could negatively affect the extensive drippage flame retardancy mechanism of NOR in polyolefins. On the other hand, nonreactive

Fig. 21 TGA data of PP, EVA, and their blend in terms of **a** weight % vs. temperature. **b** Derivative of weight % change respect to temperature vs temperature



compatibilizer provides better dispersion of flame retardant without interruption of the extensive drippage flame retardancy mechanism in the solid state, evidenced by temperature sweep rheological data. The reactive compatibilizer and NOR both increased the preferential localization of clay at the interface and in the dispersed EVA domains in the blend nanocomposite samples. In the nanocomposite samples, viscosity increased by increasing temperature, regardless of presence of reaction between NOR and compatibilizer. The increasing trend of viscosity vs temperature curves, and the decreased wettability parameter at higher temperatures were associated to the possible migration of clay platelets from interface and EVA droplets toward PP phase at elevated temperatures. Rate of clay diffusion and thus the overall viscosity of blend nanocomposites at higher temperatures were decidedly controlled by the viscosity of the surrounding medium of clay platelets, a parameter which itself was highly depended on the reaction between NOR and compatibilizer. Therefore, unlike flame-retarded blends (PP/EVA/NOR) where presence of additive reactions between NOR and compatibilizer might suppress the extensive drippage due to generation of longer/bulkier chains, in the nano clay filled-flame-retarded blends (PP/EVA/NOR/Clay), one could observe the opposite behavior, i.e., extensive drippage of blend nanocomposite samples becomes easier in the presence of additive reactions. Increased miscibility between PP and EVA at higher temperatures was the other finding made through SEM observations. It was indicated that the rheological changes at higher temperatures in EVA blends cannot be directly associated to the morphological changes; rather, it is mainly due to the degradation of EVA at those temperatures.

Acknowledgements Financial support from Ghalamchi Educational Foundation is highly appreciated. We acknowledge helpful comments from reviewers that improved the presentation of our results.

References

- Ajji A, Utracki L (1996) Interphase and compatibilization of polymer blends. *Polym Eng Sci* 36:1574–1585
- Almdal K, Koppi K, Bates F, Mortensen K (1992) Multiple ordered phases in a block copolymer melt. *Macromolecules* 25:1743–1751
- Ammar A, Elzatahry A, Al-Maadeed M, Alenizi AM, Huq AF, Karim A (2017) Nanoclay compatibilization of phase separated polysulfone/polyimide films for oxygen barrier. *Appl Clay Sci* 137:123–134
- Aznar-Aleman O, Aminot Y, Vilà-Cano J, Köck-Schulmeyer M, Readman JW, Marques A, Godinho L, Botteon E, Ferrari F, Boti V (2018) Halogenated and organophosphorus flame retardants in European aquaculture samples. *Sci Total Environ* 612:492–500
- Bagheri-Kazemabad S, Fox D, Chen Y, Geever LM, Khavandi A, Bagheri R, Higginbotham CL, Zhang H, Chen B (2012) Morphology, rheology and mechanical properties of polypropylene/ethylene–octene copolymer/clay nanocomposites: effects of the compatibilizer. *Compos Sci Technol* 72:1697–1704
- Berthier L, Chandler D, Garrahan JP (2004) Length scale for the onset of Fickian diffusion in supercooled liquids. *EPL (europhysics Letters)* 69:320
- Beyer G (2002) Nanocomposites: a new class of flame retardants for polymers. *Plastics, Additives and Compounding* 4:22–28
- Blum A, Behl M, Birnbaum LS, Diamond ML, Phillips A, Singla V, Sipes NS, Stapleton HM, Venier M (2019) Organophosphate ester flame retardants: are they a regrettable substitution for polybrominated diphenyl ethers? *Environ Sci Technol Lett* 6:638–649
- Bourbigot S, Le Bras M, Leeuwendal R, Shen KK, Schubert D (1999) Recent advances in the use of zinc borates in flame retardancy of EVA. *Polym Degrad Stab* 64:419–425
- Bousmina M (1999) Rheology of polymer blends: linear model for viscoelastic emulsions. *Rheol Acta* 38:73–83
- Camino G, Sgobbi R, Zaopo A, Colombier S, Scelza C (2000) Investigation of flame retardancy in EVA. *Fire Mater* 24:85–90
- Costache MC, Jiang DD, Wilkie CA (2005) Thermal degradation of ethylene–vinyl acetate copolymer nanocomposites. *Polymer* 46:6947–6958
- Davoodi S, Oliaei E, Davachi SM, Hejazi I, Seyfi J, Heidari BS, Ebrahimi H (2016) Preparation and characterization of interface-modified PLA/starch/PCL ternary blends using PLLA/triclosan antibacterial nanoparticles for medical applications. *RSC Adv* 6:39870–39882
- Dikobe DG, Luyt AS (2010) Morphology and thermal properties of maleic anhydride grafted polypropylene/ethylene–vinyl acetate copolymer/wood powder blend composites. *J Appl Polym Sci* 116:3193–3201
- Enescu D, Frache A, Lavaselli M, Monticelli O, Marino F (2013) Novel phosphorous–nitrogen intumescent flame retardant system. Its effects on flame retardancy and thermal properties of polypropylene. *Polym Degrad Stab* 98:297–305
- Entezam M, Khonakdar HA, Yousefi AA (2013) On the flame resistance behavior of PP/PET blends in the presence of nanoclay and a halogen-free flame retardant. *Macromol Mater Eng* 298:1074–1084
- Faker M, Aghjeh MR, Ghaffari M, Seyyedi S (2008) Rheology, morphology and mechanical properties of polyethylene/ethylene vinyl acetate copolymer (PE/EVA) blends. *Eur Polymer J* 44:1834–1842
- Feng C, Liang M, Chen W, Huang J, Liu H (2015) Flame retardancy and thermal degradation of intumescent flame retardant EVA composite with efficient charring agent. *J Anal Appl Pyrol* 113:266–273
- Friedrich C, Braun H (1992) Generalized Cole–Cole behavior and its rheological relevance. *Rheol Acta* 31:309–322
- Galbo JP, Capocci GA, Cliff NN, Detlefsen RE, DiFazio MP, Ravichandran R, Solera P, Bulliard C (2002) Hydroxy-substituted N-alkoxy hindered amines and compositions stabilized therewith. US Patent 6392041B1
- Galli P (1999) My life with polyolefin: from mountains to molecules
- Galli P, Vecellio G (2004) Polyolefins: the most promising large-volume materials for the 21st century. *J Polym Sci, Part a: Polym Chem* 42:396–415
- Goedderz D, Weber L, Markert D, Schießer A, Fasel C, Riedel R, Altstädt V, Bethke C, Fuhr O, Puchtlar F (2020) Flame retardant polyester by combination of organophosphorus compounds and an NOR radical forming agent. *J Appl Polym Sci* 137:47876
- Gomari S, Ghasemi I, Karrabi M, Azizi H (2012) Organoclay localization in polyamide 6/ethylene-butene copolymer grafted maleic anhydride blends: the effect of different types of organoclay. *J Polym Res* 19:1–11
- Goodarzi V, Jafari SH, Khonakdar HA, Monemian SA, Mortazavi M (2010) An assessment of the role of morphology in thermal/

- thermo-oxidative degradation mechanism of PP/EVA/clay nanocomposites. *Polym Degrad Stab* 95:859–869
- Graebing D, Muller R, Paliere J (1993) Linear viscoelastic behavior of some incompatible polymer blends in the melt. Interpretation of data with a model of emulsion of viscoelastic liquids. *Macromolecules* 26:320–329
- Green J (1996) Mechanisms for flame retardancy and smoke suppression—a review. *J Fire Sci* 14:426–442
- Guan Y-H, Liao W, Xu Z-Z, Chen M-J, Huang J-Q, Wang Y-Z (2015) Improvement of the flame retardancy of wood-fibre/polypropylene composites with ideal mechanical properties by a novel intumescent flame retardant system. *RSC Adv* 5:59865–59873
- Hallinan DT Jr, De Angelis MG, Giacinti Baschetti M, Sarti GC, Elabd YA (2010) Non-fickian diffusion of water in nafion. *Macromolecules* 43:4667–4678
- Hameed T, Hussein IA (2004) Effect of short chain branching of LDPE on its miscibility with linear HDPE. *Macromol Mater Eng* 289:198–203
- Han CD, Kim J (1987) Rheological technique for determining the order–disorder transition of block copolymers. *J Polym Sci, Part b: Polym Phys* 25:1741–1764
- Haurie L, Fernández AI, Velasco JI, Chimenos JM, Cuesta J-ML, Espiell F (2007) Thermal stability and flame retardancy of LDPE/EVA blends filled with synthetic hydromagnesite/aluminium hydroxide/montmorillonite and magnesium hydroxide/aluminium hydroxide/montmorillonite mixtures. *Polym Degrad Stab* 92:1082–1087
- Hemmati F, Garmabi H, Modarress H (2013) Phase behavior of UCST blends: Effects of pristine nanoclay as an effective or ineffective compatibilizer. *eXPRESS Polymer Letters* 7
- Hemmati F, Garmabi H, Modarress H (2014a) Compatibilization mechanisms of nanoclays with different surface modifiers in UCST blends: opposing effects on phase miscibility. *Polymer* 55:6623–6633
- Hemmati F, Garmabi H, Modarress H (2014b) Effects of organoclay on the compatibility and interfacial phenomena of PE/EVA blends with UCST phase behavior. *Polym Compos* 35:2329–2342
- Hemmati F, Garmabi H, Modarress H (2015) Phase behavior of polyethylene/ethylene vinyl acetate blends: Studies on miscibility window, composition dependency of interfacial interactions, and enhanced toughness. *J Plast Film Sheeting* 31:8–26
- Hoang D, Kim J (2008) Synthesis and applications of bicyclic phosphorus flame retardants. *Polym Degrad Stab* 93:36–42
- Hosseiny SM, Jafari SH, Khonakdar HA, Hemmati F, Kalaei MR (2020) A correlation between morphology and mechanical performance of injected-molded PE/EVA/clay nanocomposites: Insight into phase miscibility and interfacial phenomena. *J Appl Polym Sci* 137:49401
- Hsiue GH, Liu YL, Liao HH (2001) Flame-retardant epoxy resins: an approach from organic–inorganic hybrid nanocomposites. *J Polym Sci, Part a: Polym Chem* 39:986–996
- Hull T, Law R, Bergman Å (2014) Environmental drivers for replacement of halogenated flame retardants. *Polymer Green Flame Retardants*. Elsevier, pp 119–179
- Kapnistos M, Hinrichs A, Vlassopoulos D, Anastasiadis S, Stammer A, Wolf B (1996) Rheology of a lower critical solution temperature binary polymer blend in the homogeneous, phase-separated, and transitional regimes. *Macromolecules* 29:7155–7163
- Kiliaris P, Papaspyrides C (2010) Polymer/layered silicate (clay) nanocomposites: an overview of flame retardancy. *Prog Polym Sci* 35:902–958
- Klatt M (2014) Nitrogen-based flame retardants handbook (p179). Wiley
- Kontopoulou M, Huang LC, Lee JA (2003) Binary blends of EVA and metallocene-catalyzed ethylene- α -olefin copolymers and their film properties. *Advances in Polymer Technology: Journal of the Polymer Processing Institute* 22:209–217
- Lee HM, Park OO (1994) Rheology and dynamics of immiscible polymer blends. *J Rheol* 38:1405–1425
- Lewin M, Weil ED (2001) Mechanisms and modes of action in flame retardancy of polymers. *Fire Retardant Materials* 1:31–68
- Li Z, Qu B (2003) Flammability characterization and synergistic effects of expandable graphite with magnesium hydroxide in halogen-free flame-retardant EVA blends. *Polym Degrad Stab* 81:401–408
- Liu J, Cao D, Zhang L (2008) Molecular dynamics study on nanoparticle diffusion in polymer melts: A test of the stokes–einstein law. *The Journal of Physical Chemistry C* 112:6653–6661
- Metzler R, Klafter J (2002) From stretched exponential to inverse power-law: fractional dynamics, Cole-Cole relaxation processes, and beyond. *J Non-Cryst Solids* 305:81–87
- Murphy J (2003a) Additives for plastics handbook (chapter 10 p115–p139). Elsevier
- Murphy J (2003b) Additives for plastics handbook (chapter 8 p93–p105). Elsevier
- Nicolas RC, Wilén CE, Roth M, Pfaendner R, King RE III (2006) Azoalkanes: a novel class of flame retardants. *Macromol Rapid Commun* 27:976–981
- Nie S, Peng C, Yuan S, Zhang M (2013) Thermal and flame retardant properties of novel intumescent flame retardant polypropylene composites. *J Therm Anal Calorim* 113:865–871
- Niu Y-H, Wang Z-G (2006) Rheologically determined phase diagram and dynamically investigated phase separation kinetics of polyolefin blends. *Macromolecules* 39:4175–4183
- Park H, Park C, Tzoganakis C, Chen P (2007) Effect of molecular weight on the surface tension of polystyrene melt in supercritical nitrogen. *Ind Eng Chem Res* 46:3849–3851
- Pfaendner R (2006) How will additives shape the future of plastics? *Polym Degrad Stab* 91:2249–2256
- Picard E, Gauthier H, Gérard J-F, Espuche E (2007) Influence of the intercalated cations on the surface energy of montmorillonites: consequences for the morphology and gas barrier properties of polyethylene/montmorillonites nanocomposites. *J Colloid Interface Sci* 307:364–376
- Qian Y, Wei P, Jiang P, Zhao X, Yu H (2011) Synthesis of a novel hybrid synergistic flame retardant and its application in PP/IFR. *Polym Degrad Stab* 96:1134–1140
- Qin H, Zhang S, Zhao C, Hu G, Yang M (2005) Flame retardant mechanism of polymer/clay nanocomposites based on polypropylene. *Polymer* 46:8386–8395
- Rafiee F, Otadi M, Goodarzi V, Khonakdar HA, Jafari SH, Mardani E, Reuter U (2016) Thermal and dynamic mechanical properties of PP/EVA nanocomposites containing organo-modified layered double hydroxides. *Compos B Eng* 103:122–130
- Rault F, Giraud S, Salaün F, Almeras X (2015) Development of a halogen free flame retardant masterbatch for polypropylene fibers. *Polymers* 7:220–234
- Razavi M, Asadi V, Mehdijabbar P, Khonakdar HA, Jafari SH (2016) Application of linear rheology in determination of nanoclay localization in PLA/EVA/Clay nanocomposites: Correlation with microstructure and thermal properties. *Compos B Eng* 86:273–284
- Razavi M, Kazerouni Y, Otadi M, Khonakdar HA, Jafari SH, Ebadi-Dehaghani H, Mousavi SH (2018) A combined experimental and theoretical approach to quantitative assessment of microstructure in PLA/PP/organo-clay nanocomposites; wide-angle x-ray scattering and rheological analysis. *Composites Part B: Engineering*
- Razavi M, Khonakdar HA, Jafari SH (2015a) Application of mean-field theory in PP/EVA blends by focusing on dynamic

- mechanical properties in correlation with miscibility analysis. *Compos B Eng* 79:74–82
- Razavi M, Mardani E, Rafiee F, Otadi M, Khonakdar HA, Jafari SH, Reuter U (2017) Analysis of dynamic oscillatory rheological properties of PP/EVA/organo-modified LDH ternary hybrids based on generalized Newtonian fluid and generalized linear viscoelastic approaches. *Polym Bull* 74:465–482
- Razavi M, Nazari M, Khonakdar HA, Jafari SH, Wagenknecht U, Heinrich G (2015b) In depth analysis of micro-mechanism of mechanical property alternations in PLA/EVA/clay nanocomposites: a combined theoretical and experimental approach. *Mater Des* 88:1277–1289
- Rehage G, Ernst O, Fuhrmann J (1970) Fickian and non-Fickian diffusion in high polymer systems. *Discuss Faraday Soc* 49:208–221
- Ren Q, Xia Y, Zhang X, Zhang F, Guo J, Zhang S (2018) Synthesis of a novel flame retardant and its synergistic effect with a phosphaphenanthrene flame retardant in polypropylene/polyethylene vinyl acetate blends. *Journal of Macromolecular Science, Part B* 57:31–43
- Roe R-J (1965) Parachor and surface tension of amorphous polymers. *J Phys Chem* 69:2809–2810
- Roth M (2013) Flame retardant compositions comprising sterically hindered amines. US Patent 8349923B2
- Sain M, Park S, Suhara F, Law S (2004) Flame retardant and mechanical properties of natural fibre–PP composites containing magnesium hydroxide. *Polym Degrad Stab* 83:363–367
- Salehiyan R, Song HY, Kim M, Choi WJ, Hyun K (2016) Morphological evaluation of PP/PS blends filled with different types of clays by nonlinear rheological analysis. *Macromolecules* 49:3148–3160
- Schmitt E (2007) Phosphorus-based flame retardants for thermoplastics. *Plastics, Additives and Compounding* 9:26–30
- Seidi F, Movahedifar E, Naderi G, Akbari V, Ducos F, Shamsi R, Vahabi H, Saeb MR (2020) Flame Retardant Polypropylenes: a Review *Polymers* 12:1701
- Shao Z-B, Deng C, Tan Y, Chen M-J, Chen L, Wang Y-Z (2014) Flame retardation of polypropylene via a novel intumescent flame retardant: Ethylenediamine-modified ammonium polyphosphate. *Polym Degrad Stab* 106:88–96
- Sharma J, Clarke N (2004) Miscibility determination of a lower critical solution temperature polymer blend by rheology. *J Phys Chem B* 108:13220–13230
- Shaw SD, Blum A, Weber R, Kannan K, Rich D, Lucas D, Koshland CP, Dobraca D, Hanson S, Birnbaum LS (2010) Halogenated flame retardants: do the fire safety benefits justify the risks? *Rev Environ Health* 25:261
- Shi L (2000) Characterization of the flame retardancy of EVA copolymer by plasma grafting of acrylic acid. *Eur Polymer J* 36:2611–2615
- Sinclair KB (2001) Future trends in polyolefin materials *Macromolecular Symposia*, vol 173. Wiley Online Library, pp 237–261
- Steinmann S, Gronski W, Friedrich C (2001) Cocontinuous polymer blends: influence of viscosity and elasticity ratios of the constituent polymers on phase inversion. *Polymer* 42:6619–6629
- Szép A, Szabó A, Tóth N, Anna P, Marosi G (2006) Role of montmorillonite in flame retardancy of ethylene–vinyl acetate copolymer. *Polym Degrad Stab* 91:593–599
- Tan Y, Shao Z-B, Chen X-F, Long J-W, Chen L, Wang Y-Z (2015) Novel multifunctional organic–inorganic hybrid curing agent with high flame-retardant efficiency for epoxy resin. *ACS Appl Mater Interfaces* 7:17919–17928
- Tirri T, Aubert M, Aziz H, Brusentsev Y, Pawelec W, Wilén C-E (2019) Sulfenamides in synergistic combination with halogen free flame retardants in polypropylene. *Polym Degrad Stab* 164:75–89
- Tolinski M (2015) Additives for polyolefins: getting the most out of polypropylene, polyethylene and TPO. William Andrew
- Valera-Zaragoza M, Ramírez-Vargas E, Medellín-Rodríguez F, Huerta-Martínez B (2006) Thermal stability and flammability properties of heterophasic PP–EP/EVA/organo clay nanocomposites. *Polym Degrad Stab* 91:1319–1325
- Venier M, Salamova A, Hites RA (2015) Halogenated flame retardants in the Great Lakes environment. *Acc Chem Res* 48:1853–1861
- Vinckier I, Laun HM (1999) Manifestation of phase separation processes in oscillatory shear: droplet-matrix systems versus co-continuous morphologies. *Rheol Acta* 38:274–286
- Vlassopoulos D, Koumoutsakos A, Anastasiadis S, Hatzikiriakos S, Englezos P (1997) Rheology and phase separation in a model upper critical solution temperature polymer blend. *J Rheol* 41:739–755
- Wang G, Li W, Bai S, Wang Q (2019) Synergistic effects of flame retardants on the flammability and foamability of PS foams prepared by supercritical carbon dioxide foaming. *ACS Omega* 4:9306–9315
- Weil ED (1978) Phosphorus-based flame retardants *Flame-retardant polymeric materials*. Springer, pp 103–131
- Winter RA, Galbo JP, Seltzer R (1993) O-substituted N-hydroxy hindered amine stabilizers. US Patent 5204473A
- Wu D, Zhang Y, Zhang M, Zhou W (2008) Phase behavior and its viscoelastic response of polylactide/poly (*ε*-caprolactone) blend. *Eur Polymer J* 44:2171–2183
- Wu Q, Qu B (2001) Synergistic effects of silicotungstic acid on intumescent flame-retardant polypropylene. *Polym Degrad Stab* 74:255–261
- Xie R, Qu B (2001) Synergistic effects of expandable graphite with some halogen-free flame retardants in polyolefin blends. *Polym Degrad Stab* 71:375–380
- Yang S, Zhang Q, Hu Y (2016) Synthesis of a novel flame retardant containing phosphorus, nitrogen and boron and its application in flame-retardant epoxy resin. *Polym Degrad Stab* 133:358–366
- Yen Y-Y, Wang H-T, Guo W-J (2012) Synergistic flame retardant effect of metal hydroxide and nanoclay in EVA composites. *Polym Degrad Stab* 97:863–869
- Yu L, Chen L, Dong L-P, Li L-J, Wang Y-Z (2014) Organic–inorganic hybrid flame retardant: preparation, characterization and application in EVA. *RSC Adv* 4:17812–17821
- Zhang Q, Leroux F, Tang P, Li D, Feng Y (2018) Low molecular weight hindered amine light stabilizers (HALS) intercalated MgAl-Layered double hydroxides: Preparation and anti-aging performance in polypropylene nanocomposites. *Polym Degrad Stab* 154:55–61
- Zhao W, Hu Q, Zhang N, Wei Y, Zhao Q, Zhang Y, Dong J, Sun Z, Liu B, Li L (2017) In situ inorganic flame retardant modified hemp and its polypropylene composites. *RSC Adv* 7:32236–32245
- Zwanzig R, Harrison AK (1985) Modifications of the Stokes-Einstein formula. *J Chem Phys* 83:5861–5862

Publisher's note Springer Nature remains neutral with regard to jurisdictional claims in published maps and institutional affiliations.